

# 5

## LEO Coverage

### 5.1 LEO Coverage Concept

The low Earth orbiting (LEO) satellite's coverage area represents the fraction of the Earth's surface from where users have visibility with satellite, can access and establish communication with satellite. Users (stations) on the ground can communicate with LEO satellites when the user (station) is under the coverage area (satellite footprint) as presented in [Figure 5.1](#). Since the satellite is always on the move, the coverage area moves also, so that at various points the user is out of the footprint, and consequently loses communication. Visibility duration and consequently communication duration varies for each LEO satellite pass over the ground station, since LEO satellites move quickly over the Earth, several times during the sidereal daytime. The satellite's coverage area is usually expressed as a percentage of the Earth's surface, which is really a low percentage for LEO satellites – just a few percent of Earth's area.

The coverage area of a single satellite is a circular area ([Figure 5.1](#)) on the Earth's surface from where the satellite can be seen under an elevation angle equal to or greater than the minimum elevation angle determined by the system/mission requirements. The largest coverage area of a LEO single satellite is achieved under the elevation of  $\varepsilon_0 = 0^\circ$ , which is not always provided because of natural/artificial barriers under too-low elevation. The single LEO satellite coverage aspects serve as an overture to the global coverage.

Often there is confusion between the coverage area and the ideal/designed horizon plane. The ideal horizon plane is the virtual flat surface

laid perpendicularly on Earth's radius vector ([Figure 1.21](#) or [4.12](#)), where the radius vector connects the Earth's center with the ground station within the satellite's coverage area. On the other hand, the coverage area is spherical area on the ground, where each point within that area has its own horizon plane, providing different view of the satellite. Thus, within the satellite's coverage area, each user has its own ideal/designed horizon plane, so each user on the ground has different communication line with the single satellite. The designed horizon plane is simply the parallel with the ideal one distanced from it by the distance ( $L_{DHPW}$ ) determined by the designed elevation angle (see [Eq. 4.28](#)).

The satellite is looking down at its coverage area for the user to be locked and communicate, and on the other side the user is looking up at its own horizon plane for the satellite to be locked for the communication.

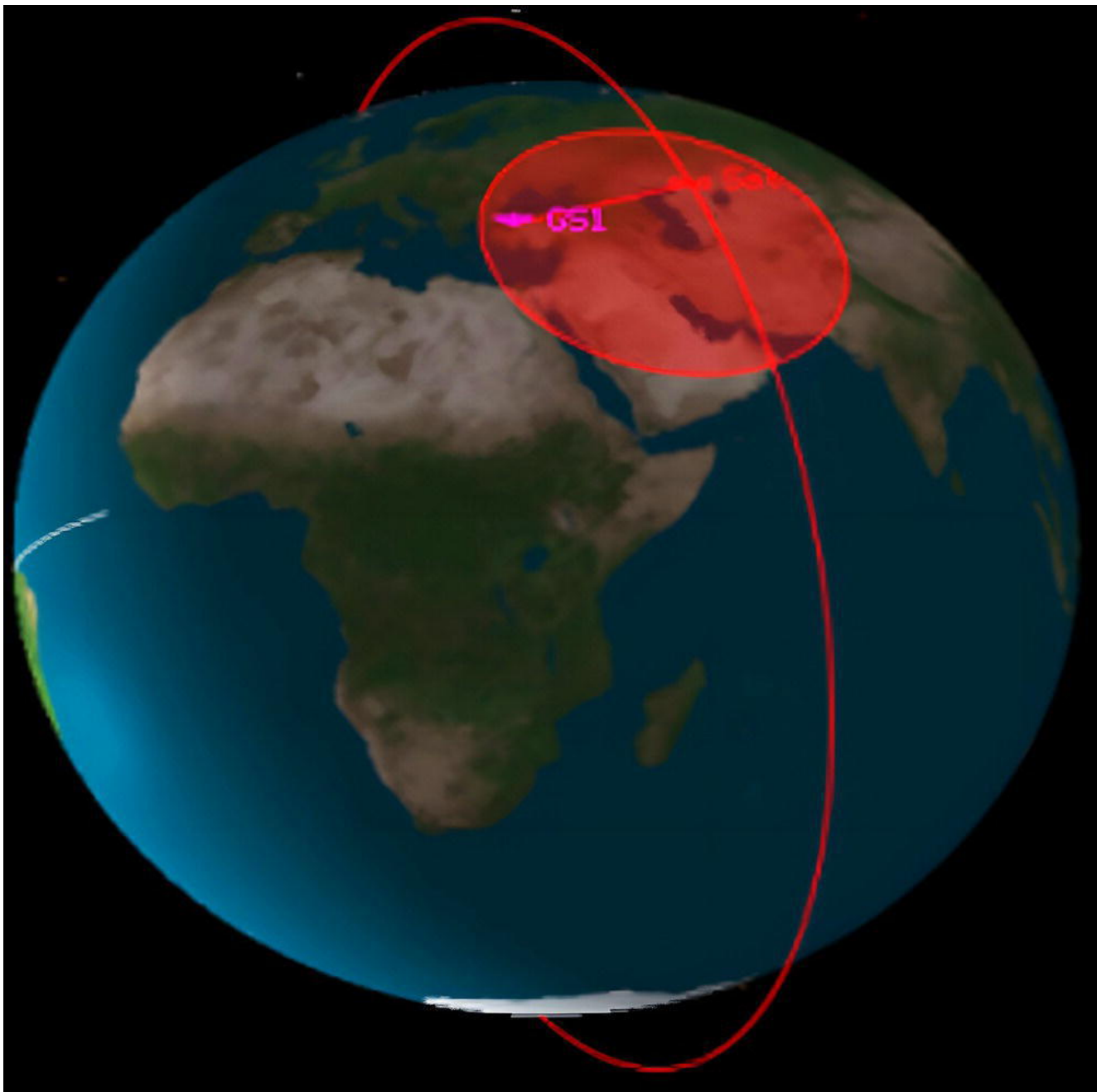


**Figure 5.1** The ground station (GS) under the LEO coverage area.

## 5.2 LEO Coverage Geometry

For the further mathematical calculation, the geometry description is applied. The coverage geometry for LEO satellites is given in [Figure 5.2](#). The LEO satellite is orbiting above the Earth at altitude  $H$ . In [Figure 5.2](#) two coverage cases are given: the first one, the largest (full) coverage is under the elevation of  $\varepsilon_0 = 0^\circ$  and the second one is under the predetermined elevation, or better expressed under the designed

elevation. There are two triangles in [Figure 5.2](#). The largest triangle is related to the largest (full) coverage, which is given by the larger circle. The smaller triangle is related to the LEO coverage area on the Earth's surface under a few degrees of elevation (predefined elevation-designed elevation) given in the figure by the smaller circle. For both triangles:  $\varepsilon_0$  is elevation angle,  $\alpha_0$  is nadir angle,  $\beta_0$  is central angle, and  $d$  is the slant range.  $R_E = 6371 \text{ km}$  is the Earth's radius. Generally, for triangles, it is:

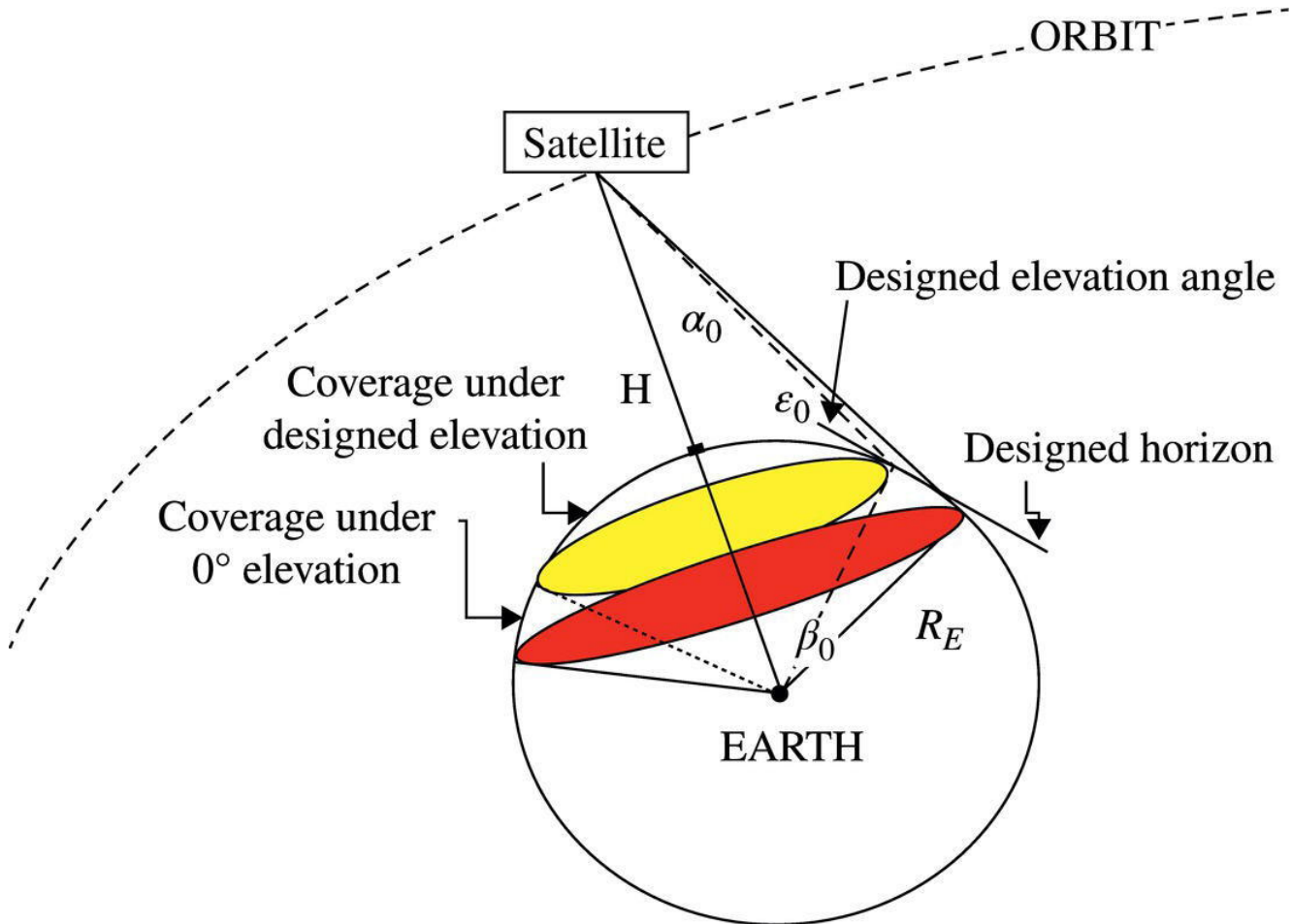


[Figure 5.2](#) LEO coverage area geometry.

$$(\varepsilon_0 + 90^\circ) + \alpha_0 + \beta_0 = 180^\circ \quad (5.1)$$

Since the ideal horizon plane is always perpendicular with Earth's radius vector, this yields:

$$\varepsilon_0 + \alpha_0 + \beta_0 = 90^\circ \quad (5.2)$$

Furthermore, applying the sinus theorem:

$$\frac{\sin \alpha_0}{R_E} = \frac{\sin (90 + \varepsilon_0)}{R_E + H} \quad (5.3)$$

$$\sin \alpha_0 = \frac{R_E}{R_E + H} \cos \varepsilon_0 \quad (5.4)$$

The full coverage is achieved for  $\varepsilon_0 = 0$ , and this condition determines the largest nadir angle of the satellite's propagation toward the Earth:

$$\alpha_{0, max} = \sin^{-1} \left( \frac{R_E}{R_E + H} \right) \quad (5.5)$$

By definition, the coverage  $C$  [%] is the fraction of the Earth's surface covered by the satellite, expressed as the ratio of the satellite coverage area ( $SAT_{COVERAGE}$ ) to the Earth's surface ( $S_{EARTH}$ ) as:

$$C [\%] = \frac{SAT_{COVERAGE}}{S_{EARTH}} \quad (5.6)$$

From (Richharia, [1999](#); Roddy [2006](#)), or even from elementary geometry it is:  $SAT_{COVERAGE} = 2\pi R_E^2 (1 - \cos \beta_0)$  and  $S_{EARTH} = 4\pi R_E^2$ , thus the coverage area by LEO satellite expressed in percentage is:

$$C [\%] = \frac{1}{2} (1 - \cos \beta_0) \quad (5.7)$$

The satellite's coverage area of Earth depends on orbital parameters – more accurately, the coverage as a percentage value or as a surface expressed in square kilometers depends on altitude and elevation angle, but as a position on Earth's surface also depends on inclination.

### 5.3 The Coverage of LEO Satellites at Low Elevation

The largest coverage area is achieved under elevation of  $0^\circ$ , but the lock and unlock between the satellite and the appropriate ground station

under this elevation is too difficult to establish because of the natural/artificial barriers. That is, the line of site between the satellite and the ground station is hindered by natural/artificial obstacles interfering with the communications. To avoid such obstacles at too-low elevation, usually a designed elevation angle is determined. But, under the designed elevation, the coverage area decreases, which leads to the compromise to be applied for the link budget calculations.

**Idea:** The idea is to draw conclusions about the reliability in communication between the satellite and the ground station under too low elevation. More exactly, it is to define the elevation angle, which provides the safe and reliable communication and its impact on the coverage area width, and consequently, on the range between the satellite and the ground station. The determined range is the crucial component for the appropriate link budget calculations.

**Method:** Simulation and math calculations are applied. For the coverage area analysis under too-low elevation, the basic geometry between a satellite and ground station is applied, where ( $\alpha_0$ ) is nadir angle, ( $\beta_0$ ) is central angle, and ( $\varepsilon_0$ ) is elevation angle. For simulation purposes, the altitudes from 600 km up to 1200 km are considered. Since the satellite's coverage strongly depends on elevation angle, also for the simulation purposes, it is considered the elevation up to  $10^\circ$ , elevated by steps of  $2^\circ$  (Cakaj et al., [2014](#)). For a given satellite altitude  $H$  and a given elevation angle  $\varepsilon_0$  should first be calculated  $\alpha_0$ , from [Eq. \(5.4\)](#) and then  $\beta_0$  from [Eq. \(5.2\)](#). Finally, the coverage area expressed in percentage is calculated based on [Eq. \(\(5.7\)\)](#). For altitudes of  $H = 600$  km, 800 km, 1000 km, and 1200 km, which are typical low-orbit attitudes, it is simulated and calculated the coverage area for the elevation of  $(0\text{--}10)^\circ$  by steps of  $2^\circ$ .

**Results:** Under the previous simulation assumptions, the results are presented in [Table 5.1](#) and [Figure 5.3](#) (Cakaj et al., [2014](#)).

[Table 5.1](#) and [Figure 5.3](#) confirm the decrease of coverage area as elevation angle increases for the already defined altitude  $H$ , and the

increase of the coverage area as altitude  $H$  increases, keeping the elevation fixed.

Finally, [Figure 5.4](#), applying satellite orbit analysis software, presents the case of simulated coverage area for synchronized orbits at an altitude of 600 km for different inclination (few orbits) at elevation of  $10^\circ$ , as the smallest coverage area stems from the simulation previously considered. Small circles in [Figure 5.4](#) represent LEO coverage area on Earth's surface.

**Conclusions:** Satellite coverage strongly depends on elevation angle. The largest coverage area is achieved under elevation of  $0^\circ$ , but in order to avoid obstacles caused by natural barriers at too-low elevation, usually for the link budget calculations, the minimal elevation angle is determined, which ranges from  $2^\circ$  to  $10^\circ$ .

Through simulation for typical LEO attitudes on range of 600–1200 km at low elevation of  $0^\circ$  to  $10^\circ$ , it is confirmed that the fraction of Earth covered by satellites at appropriate attitudes is 1.69% to 7.95%.

**Table 5.1** Coverage areas as a fraction of Earth area.

Orbital Attitude [km]	H 600 [km]	H 800 [km]	H 1000 [km]	H 1200 [km]
Elevation ( $\varepsilon_0$ )	Coverage [%]	Coverage [%]	Coverage [%]	Coverage [%]
$0^\circ$	4.30	5.60	6.80	7.95
$2^\circ$	3.63	4.84	5.95	7.08
$4^\circ$	3.05	4.16	5.21	6.22
$6^\circ$	2.53	3.49	4.54	5.48
$8^\circ$	2.08	3.01	3.91	4.75
$10^\circ$	1.69	2.54	3.38	4.20



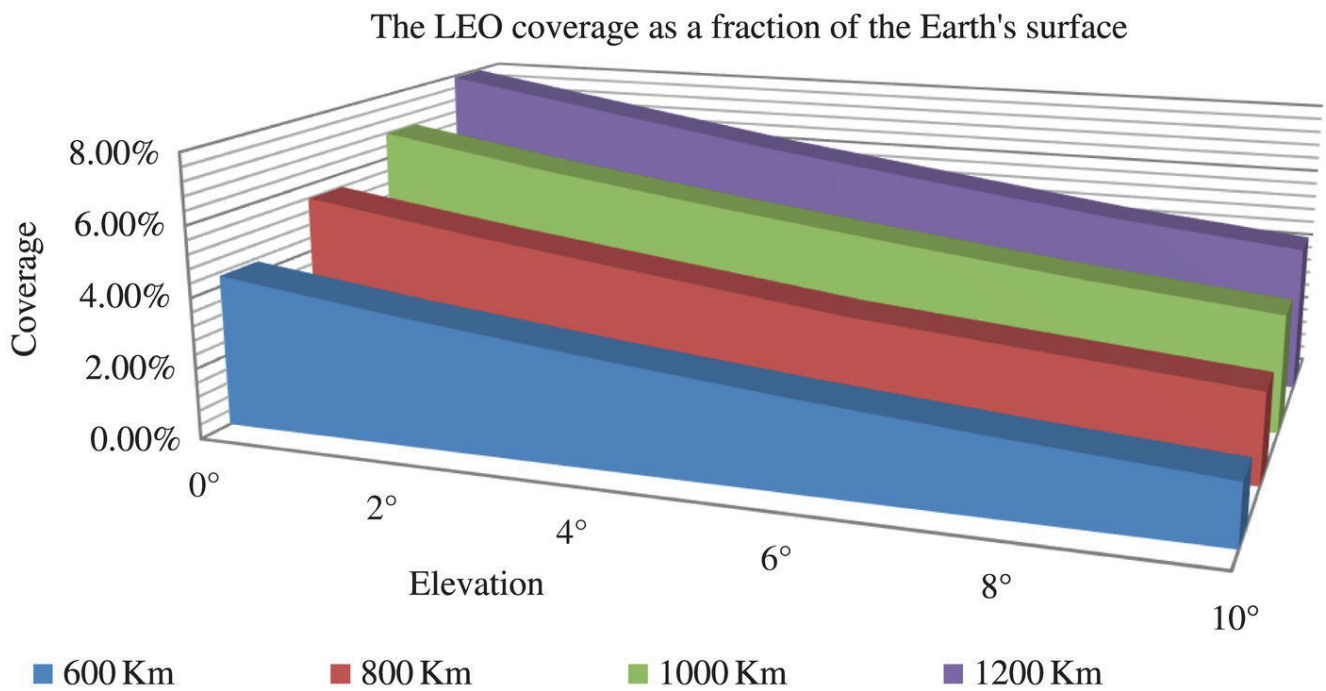


**Figure 5.3** Coverage area variation for different altitudes at low elevation.

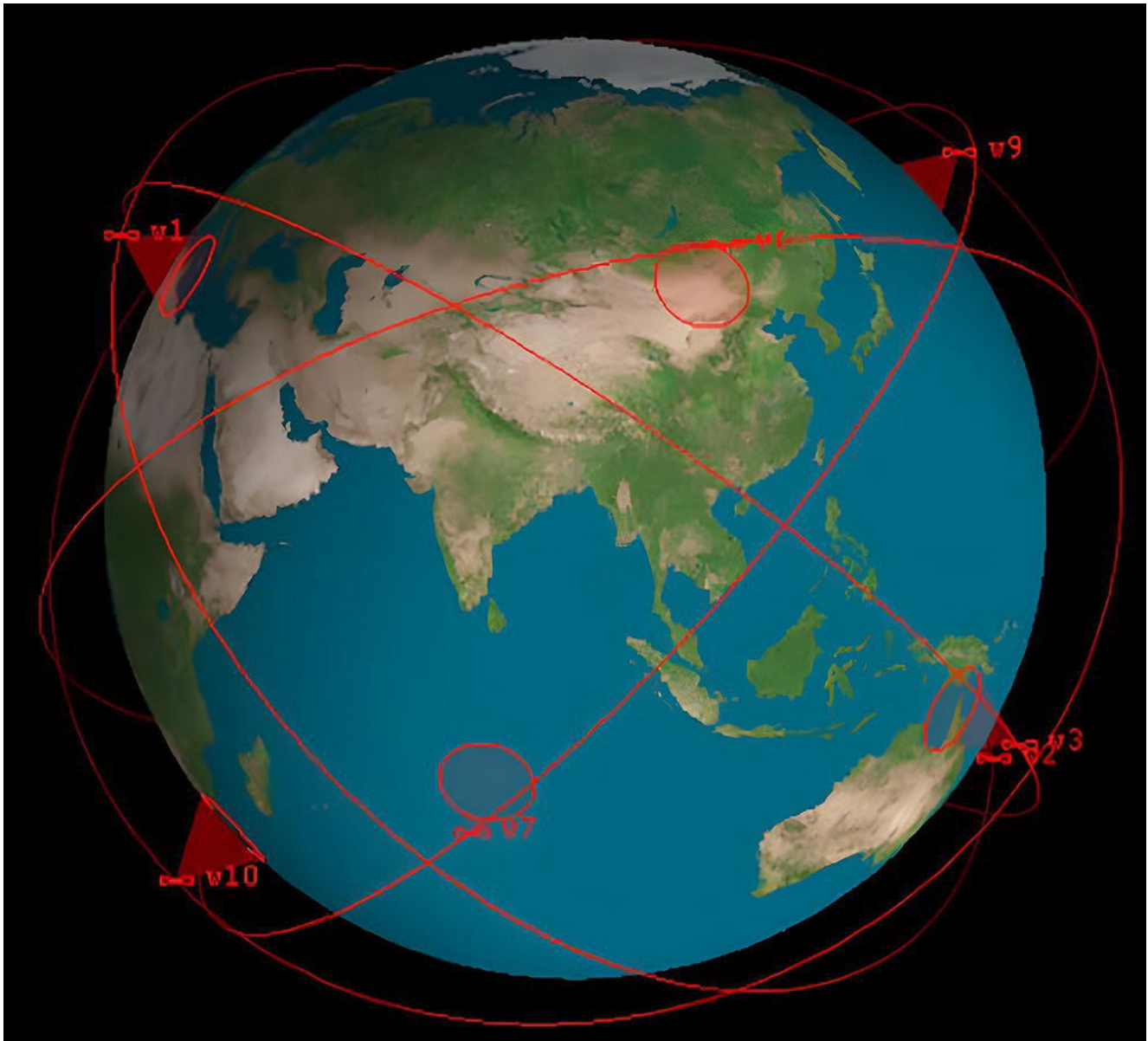


**Figure 5.4** LEO coverage area.

## 5.4 Coverage Belt

The LEO satellite orbit is in principle fixed and the satellite flies strongly keeping its path determined by Kepler elements (if no disturbances). Thus, as the satellite orbits around the Earth, consequently the coverage area on Earth under the satellite, also virtually moves vertically, as presented in [Figure 5.5](#). The Earth's area swept by LEO satellite's coverage during one orbit path is known as a coverage belt as given in [Figure 5.6](#). The width of the appropriate coverage belt depends on satellite altitude.

Satellites under the same altitude but under different inclination make different belts, enabling global coverage, but not instant one.

As the coverage area virtually moves vertically, the Earth rotates horizontally around its N-S axis (Roddy, [2006](#)), as shown in [Figure 5.7](#). As the Earth rotates eastward, the coverage belt virtually moves westward, providing access to the satellite from each point on Earth, but not at the same (provided by author's time at NOAA on 2009). A single satellite can provide global access, but not simultaneously, thus a single one cannot provide continuous real-time services. Single-satellite coverage is known as an *individual* satellite coverage. For continuous service, however, a satellite constellation should be considered.

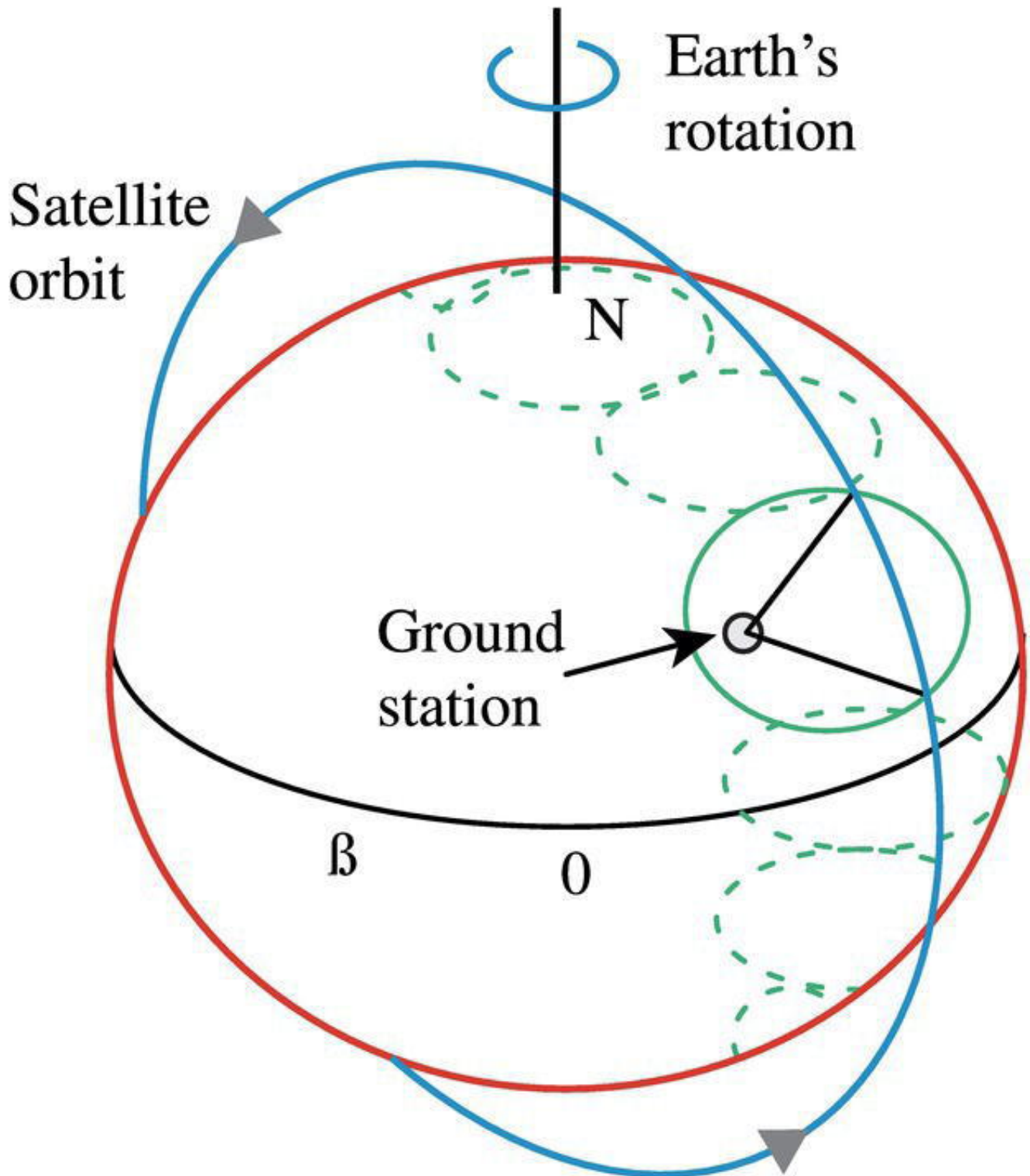


**Figure 5.5** Virtual coverage movement.

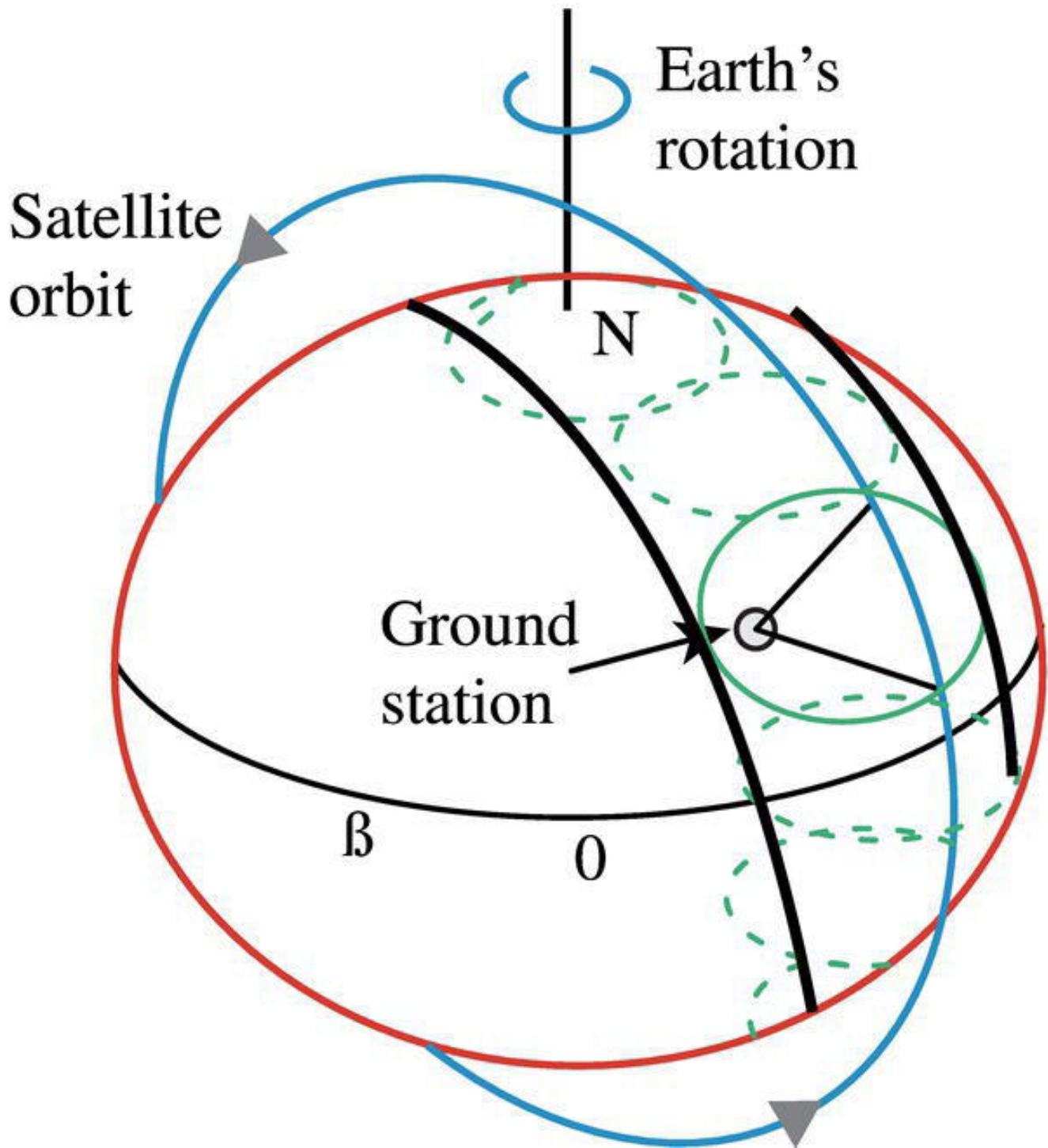


**Figure 5.6** Coverage belt.

**Idea:** What is the width of the appropriate coverage belt? This is further elaborated!

**Method:** Simulation and math calculations are applied. Let us assume a ground station at the center of the coverage area. The distance  $d$  between the ground station and the satellite, under elevation of  $0^\circ$  (apply [Eq. \(1.56\)](#)), represents the radius of the largest coverage area's circle. The

width of the coverage belt is twice that of the largest radius, expressed as follows:

$$d_{(\varepsilon_0 = 0)} = d_{max} = R_E \left[ \sqrt{\left( \frac{H + R_E}{R_E} \right)^2 - 1} \right] \quad (5.8)$$

$$D_{BELT} = 2d_{max} \quad (5.9)$$

Based on [Eq. \(5.8\)](#) and [Eq. \(5.9\)](#), it is obvious that the satellite coverage belt strongly depends on altitude and elevation angle. The largest one is under elevation of  $0^\circ$ . To conclude about the coverage belt variation for low orbiting satellites, the simulation for altitudes from 600 km up to 1200 km is further applied, as illustrated by [Figure 5.8](#). Schematically in [Figure 5.8](#) is presented the belt wideness variation for two different satellites SAT1 and SAT2, under different altitudes  $H1$  and  $H2$  (Cakaj, [2016](#)). For altitudes of  $H = 600$  km, 800 km, 1000 km, and 1200 km, which are typical low-orbit altitudes, we simulate and calculate the coverage belt width for elevations of  $(0\text{--}10)^\circ$  by steps of  $2^\circ$ .

**Results:** The results are presented in [Table 5.2](#) and [Figure 5.9](#), which confirm the decrease of coverage belt width as the elevation angle increases for the already defined altitude  $H$ , and the increase of the coverage belt width as altitude  $H$  increases under the fixed elevation.

**Conclusions:** The satellite's coverage belt on the Earth depends strongly on orbit altitude and elevation angle. The widest coverage belt is achieved under elevation of  $0^\circ$ , but in order to avoid obstacles caused by natural barriers at too-low elevation, usually for the link budget calculations, the minimal elevation angle ranges from  $2^\circ$  to  $10^\circ$ . For the higher elevation consequently the narrower coverage belt is generated. Through simulation for typical LEO attitudes of 600–1200 km, it is confirmed that the coverage belt width covered by satellites at respective altitudes ranges from 5633 to 8177 km.

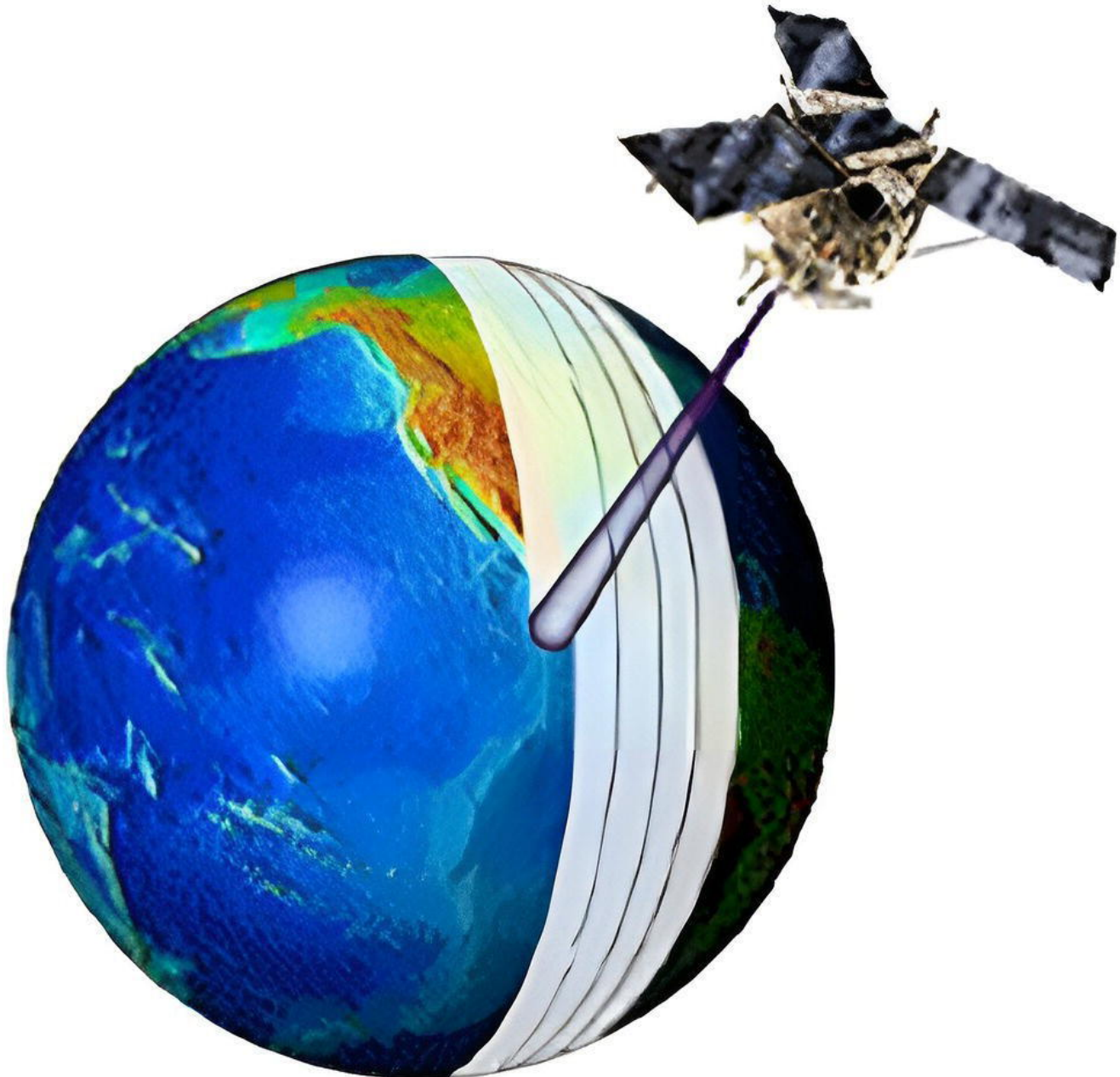


**Figure 5.7** LEO coverage belt.

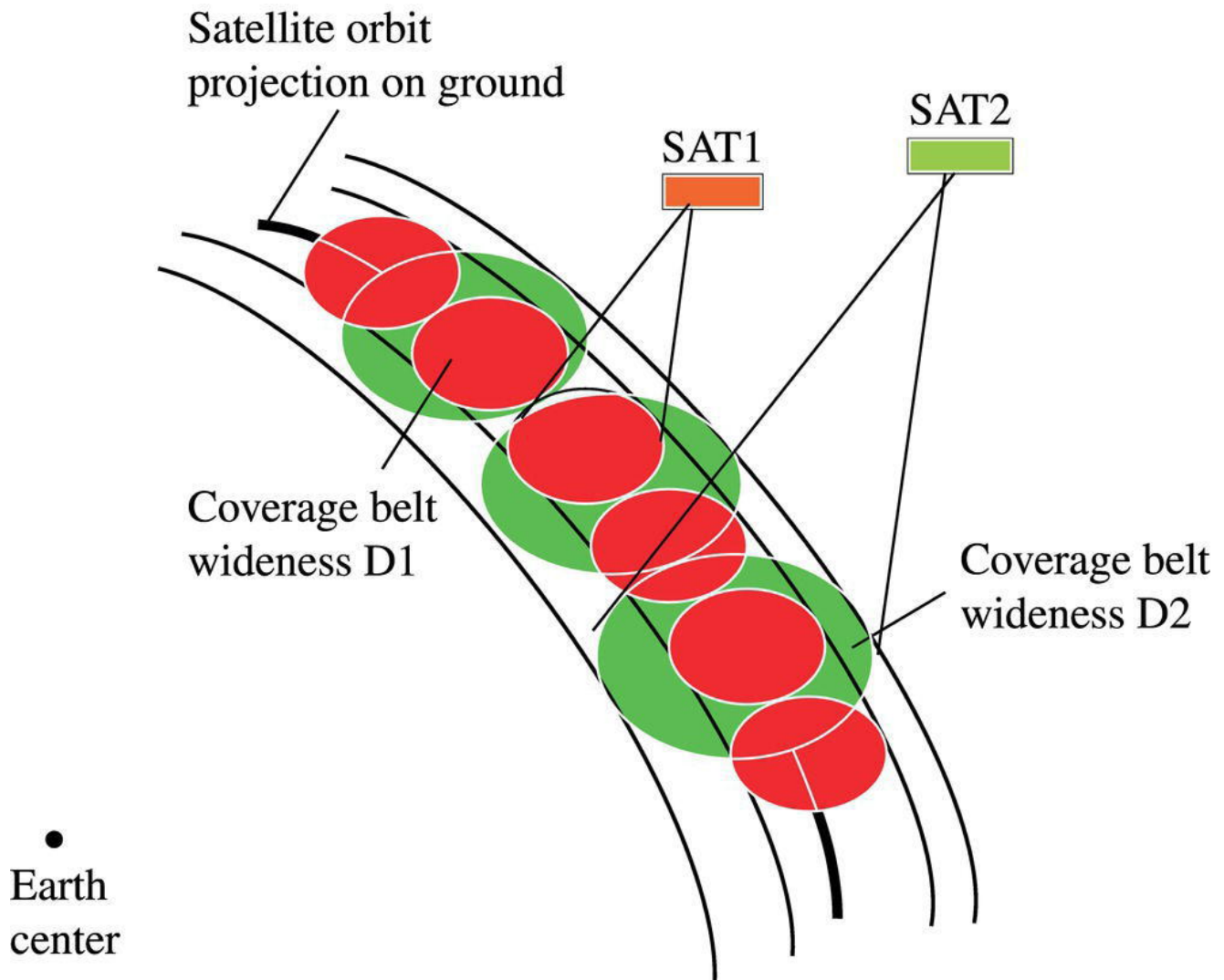


**Figure 5.8** Coverage belt of different satellite altitudes.

## 5.5 LEO Global Coverage

Recently, LEO satellites are oriented on providing real-time continuous services, what implies the necessity for the global coverage and handover process. The global satellite coverage can be considered as an interoperable complementary networking process of multiple satellites organized in a constellation, each of them contributing with its individual coverage (Zong and Kohani, [2019](#); Seyed and Safavi, [2012](#)). Let us first discuss the individual coverage and then the necessity for other satellites involvement (creating constellation) for the global coverage.

**Table 5.2** Coverage belt width.

<b>Orbital Attitude [km]</b>	<b>H 600 [km]</b>	<b>H 800 [km]</b>	<b>H 1000 [km]</b>	<b>H 1200 [km]</b>
<b>Elevation (<math>\varepsilon_0</math>)</b>	<b>D [km]</b>	<b>D [km]</b>	<b>D [km]</b>	<b>D [km]</b>
0°	5633.0	6579.0	7416.0	8177.8
2°	5215.2	6157.2	6991.4	7751.2
4°	4824.4	5760.2	6590.6	7347.2
6°	4463.0	5386.8	6210.0	6959.8
8°	4141.6	5048.8	5859.2	6601.2
10°	3857.4	4745.0	5541.8	6273.6

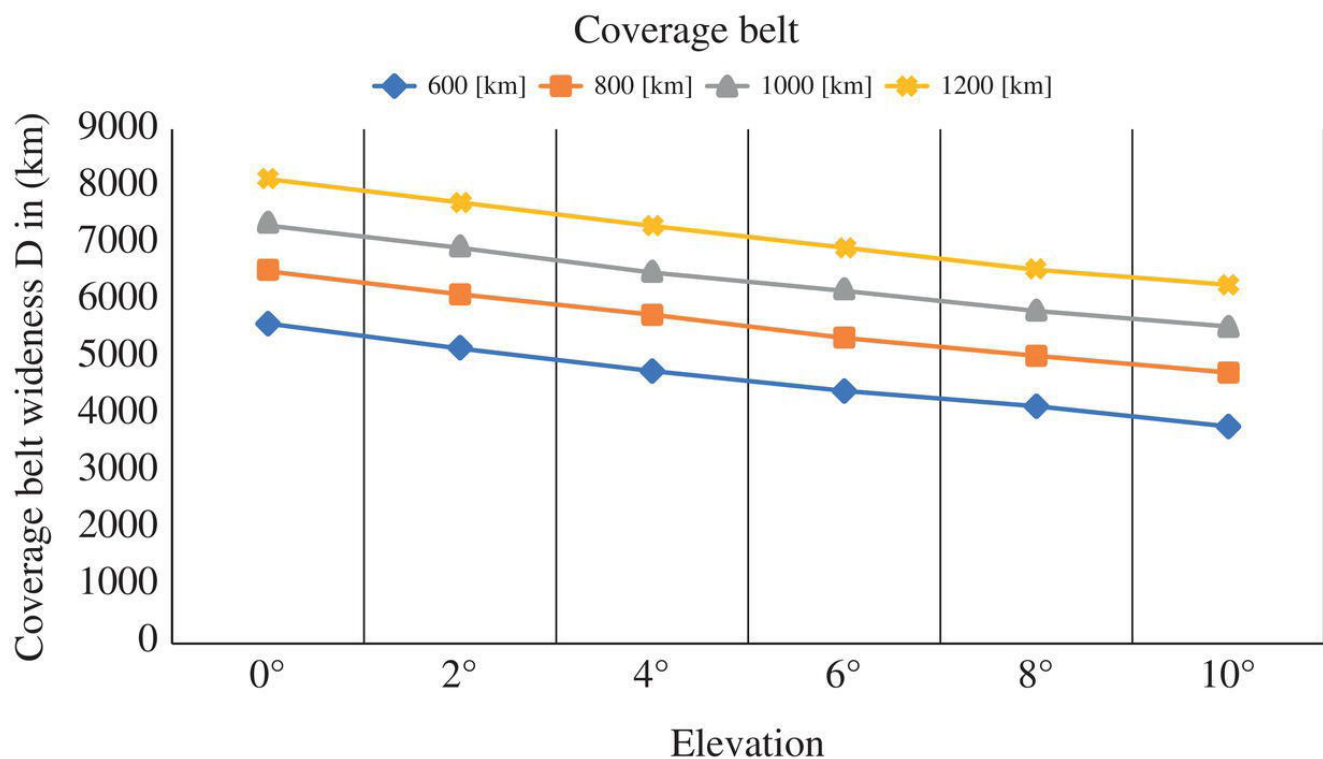


**Figure 5.9** Coverage belt variation for different altitudes at low elevation.

The simulated coverage area based on the LEO satellite orbital parameters is given in [Figure 5.10](#). (Cakaj, 2021). The altitude applied for simulation is 800 km. The user on ground (defined as LUTKOS for simulation purposes) is locked with a LEO satellite since it is under coverage area (satellite footprint). The lock is symbolized with the line connecting the

LUTKOS and the satellite SAT (Cakaj, [2010](#)). For simulation purposes and coverage interpretation, four more basic communication points (BC) are given, as BC1, BC2, BC3, and BC4.

Under the case presented in [Figure 5.10](#), only two of them (BC1 and BC4) can be locked with the satellite since they are within satellite's footprint, and two others (BC2 and BC3) are out of the footprint, so with no communications possibility. This means that BC1 and BC4 can communicate with each other via satellite, but not with BC2 and BC3 since the last ones are not accessible by satellite. This is known as ***communication within coverage area*** (footprint), or as ***individual satellite coverage***. As the satellite moves down in its orbit, the coverage area also vertically moves, leaving the ground station (LUTKOS) and two base stations (BC1, BC4) out of the footprint and consequently losing the communication (Cakaj et al., [2014](#)).



**Figure 5.10** Simulated LEO satellite's coverage area.

Let us further suppose the second LEO satellite with the same altitude is orbiting the Earth as shown in [Figure 5.10](#). Since, both have the same altitude, the dimensions of the satellite area are the same, just covering different zones. Let us suppose that coverage areas are adjacent, so the second satellite is covering basic communication points BC2 and BC3. This means that BC2 and BC3 can communicate with each other intermediated by the second satellite, but no one of them with BC1

and BC4 since the last ones are not accessible by the second satellite. If the first and second satellite can communicate with each other, these satellites will enable the communication among all four basic communication points. This is interoperability complementary process by two satellites providing communications within two coverage areas. This concept – step by step, adding more satellites, to build an organized ***satellite constellation*** – provides global coverage. The Iridium satellite constellation system is among the earliest systems providing global coverage planned to provide worldwide communication services, shown in [Figure 5.11](#) (Jong et al. [2014](#)).

LEO satellites organized in constellations act as a convenient network solution for global coverage and real-time services (Zong and Kohani, [2019](#); Seyed and Safavi, [2012](#)). The LEO constellation is a system of LEO identical satellites, launched in several orbital planes with the orbits having the same altitude (single-layer constellation). The satellites move in a synchronized manner in trajectories relative to Earth. Satellites in low orbits arranged in a constellation work together by relaying information to each other and to the users on the ground. Each individual satellite of constellation contributes with its coverage, toward global coverage created by interoperability. The application of LEO satellites organized in a ***constellation*** is an alternative to wireless telephone networks.

Global coverage should be so smooth that the user does not detect that the signal is being handed over from one satellite to another (Seyed and Safavi, [2012](#)). Handover and management policies become even more critical under very low elevation because of natural barriers. Handover policies and management are well analyzed (Alyildiz et al. [1999](#); Papapetrou et al. [2003](#)).

The handover process is highly risky at these low elevations; thus, for complete coverage of the Earth's surface, some overlap between adjacent satellites is necessary so that users on the ground do not sense any lack

of continuity in real-time services. Usually, the coverage areas overlap by few degrees. Overlapping of the satellite constellation is given in [Figure 5.12](#) (Xiao et al. 2018). The handover process is executed within the overlapped area. The satellites within a constellation are equipped with advanced on-board processing; they can intercommunicate with each other by line of sight using intersatellite links (ISL), applied for the handover process and intersatellite traffic.

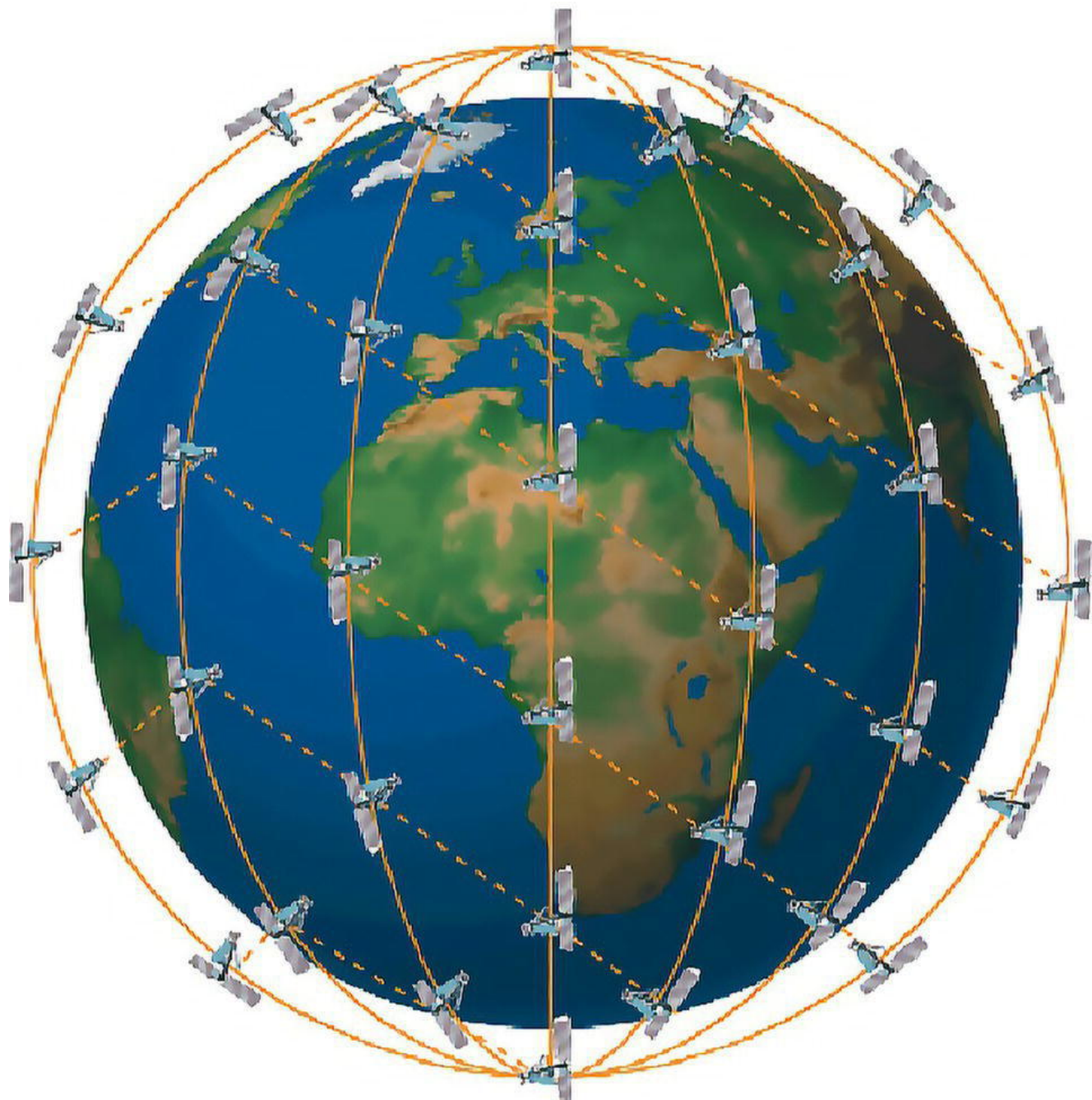


**Figure 5.11** Iridium constellation.

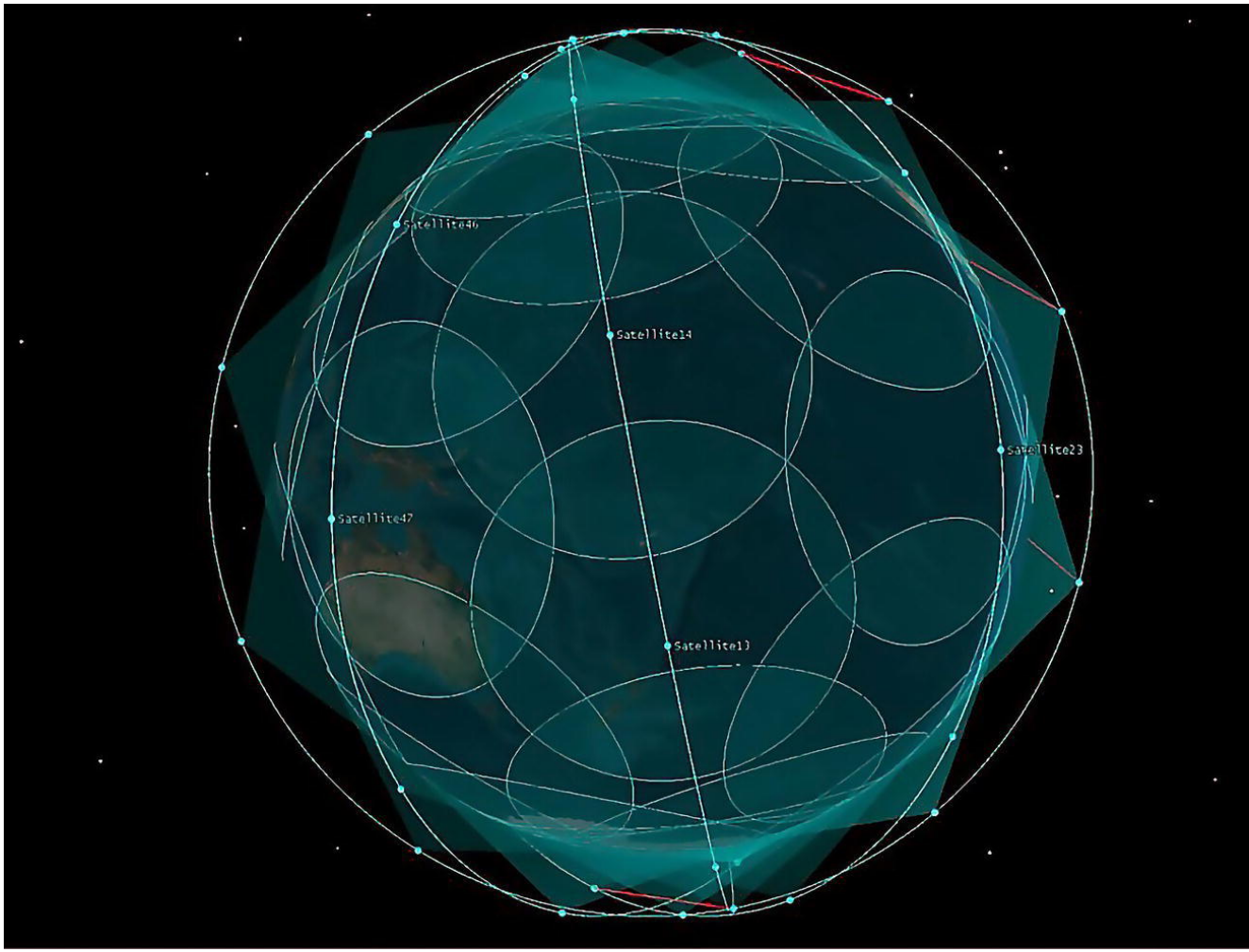


**Figure 5.12** LEO overlapped coverage area (Xiao et al. [2018](#)).

When designing a satellite network some decisions such as the selection of the orbit parameters, coverage model, the network connectivity and routing model must be made. Different deterministic models for coverage time evaluation of LEO satellite are developed. Models involve statistical coverage time assessments. The analyses are particularly useful for probabilistic investigation of intersatellite handovers in LEO satellite networks (Papapetrou et al. [2003](#)). The probability of service interruption and handover mechanism becomes important for the overall system performance (Seyedi and Safavi, [2012](#)).

## 5.6 Constellation's Coverage – Starlink Case

Technological efforts toward an integrated satellite-terrestrial network stem by the end of the last century, especially with the applications

of LEO microsatellites and nanosatellites. Integrated satellite-terrestrial networking toward providing global internet broadband services recently reflects the highest research scientific and industry interests worldwide. Active satellite projects related to an integrated satellite-terrestrial communication network include Iridium constellation with 66 satellites (Cochetti, [2015](#)), OneWeb constellation with 648 satellites (De Selding, [2015](#); Pultarova and Henry, [2017](#)), and Telesat with 117 spacecrafts in its constellation (Foust, [2018](#)). The Federal Communications Commission (FCC) has approved Amazon's plan to launch 3236 spacecraft in its Kuiper constellation, but the largest undertaking is the Starlink satellite constellation, coming from SpaceX, a private US company majority owned by Elon Musk (Starlink, [2020](#); Starlink Satellite Missions, [2020](#)).

The Starlink constellation is planned to be organized in three spatial shells, each of them with several hundred small-dimensioned and lightweight LEO satellites specially designed to cover the entire Earth with broadband services through a satellite-terrestrial integrated network, connecting ground stations with 4,425 LEO satellites.

As of October 24, 2020, 893 satellites were accommodated in orbits of altitude of 550 km under different inclinations, determining the first Starlink orbital shell. Two next generations are planned for altitudes of 1110 and 340 km, completing the appropriate infrastructure of three Starlink satellite shells, toward ubiquitous presence of broadband internet services (Cakaj, [2021](#)).

Nearly 12 000 satellites are planned to be deployed, organized in three orbital shells, as follows (Starlink, [2020](#); Starlink Satellite Missions, [2020](#)):

- The first shell: 1440 satellites in a 550 km altitude.
- The second shell: 2825 satellites in a 1110 km altitude.
- The third shell: 7500 satellites in 340 km altitude.

The first shell of 1440 satellites will be into 72 orbital planes of 20 satellites each, and others later by intention to be completed by 2024 and to provide real-time broadband services (Starlink, [2020](#); Starlink Satellite Missions, [2020](#)). [Figure 5.13](#) presents a train of SpaceX Starlink satellites visible and captured by satellite tracker Marco Langbroek in Leiden, the Netherlands, on May 24, 2019 (Rao, [2019](#)).

**Idea:** These three satellite's orbital shells manifest different coverage on Earth because of their different altitudes. Here we want to compare three shells under different elevation.



[Figure 5.13](#) Starlink satellite train.

**Method:** The coverage area calculation under [section 5.2](#) is applied. For the Starlink constellation, considering three shells at altitudes  $H = 550$ ,  $1110$ , and  $340$  km for the full coverage under elevation of  $\epsilon_0 = 0$  and for the designed elevation  $\epsilon_{0D} = 25^\circ, 30^\circ, 35^\circ, 40^\circ$  based on [Eq. \(5.2\), \(5.4\)](#) are

calculated nadir angle  $\alpha_0$ ° and central angle  $\beta_0$ ° as the first step for the coverage calculation for all three Starlink shells. Then, applying the above calculated  $\beta_0$ ° and considering three shells at altitudes  $H = 550, 1110$ , and  $340$  km for the full-coverage elevation of  $\varepsilon_0 = 0$  and for the designed elevation  $\varepsilon_{0D} = 25^\circ, 30^\circ, 35^\circ, 40^\circ$  based on [Eq. \(\(5.7\)\)](#), the respective coverage for all three Starlink shells is calculated ([Cakaj, 2021](#)).

**Results:** The mathematical outcomes are presented in [Table 5.3](#) and [Table 5.4](#).

**Conclusions:** The too-low fraction of the Earth's surface covered by LEO satellites, even without overlapping, justifies the large number of satellites in constellation to be applied, to ensure the safe communication and the real-time continuity of services. Earth's surface area is  $510$  million km $^2$ ; thus, the LEO satellite at altitude of  $550$  km under elevation of  $40^\circ$ , covers the area of  $0.00206 \times 510$  million km $^2 = 1.05$  million km $^2$ , which is in fact the circled area on Earth with approximately radius of  $580$  km.

[Table 5.3](#) Nadir angle and central angle for different elevations.

The horizon plane elevation ( $\varepsilon_0$ )	The first shell $H = 550$ km		The second shell $H = 1110$ km		The third shell $H = 340$ km	
	$\alpha_0$ (°)	$\beta_0$ (°)	$\alpha_0$ (°)	$\beta_0$ (°)	$\alpha_0$ (°)	$\beta_0$ (°)
Ideal: $0^\circ$	<b>66.9</b>	<b>23.1</b>	<b>58.3</b>	<b>31.7</b>	<b>71.6</b>	<b>18.4</b>
Designed at: $25^\circ$	<b>56.4</b>	<b>8.6</b>	<b>50.4</b>	<b>14.6</b>	<b>59.3</b>	<b>5.7</b>
Designed at: $30^\circ$	<b>52.8</b>	<b>7.2</b>	<b>47.5</b>	<b>12.5</b>	<b>55.2</b>	<b>4.8</b>
Designed at: $35^\circ$	<b>48.9</b>	<b>6.1</b>	<b>44.2</b>	<b>10.8</b>	<b>51.0</b>	<b>4.0</b>
Designed at: $40^\circ$	<b>44.8</b>	<b>5.2</b>	<b>40.7</b>	<b>9.3</b>	<b>46.6</b>	<b>3.4</b>



[Table 5.4](#) Coverage of the Starlink satellites.

The horizon plane elevation ( $\varepsilon_0$ )	The first shell $H = 550$ km	The second shell $H = 1110$ km	The third shell $H = 340$ km
	$C [\%]$	$C [\%]$	$C [\%]$
Ideal: $0^\circ$	4.003	7.461	2.55
Designed at: $25^\circ$	0.560	1.614	0.247
Designed at: $30^\circ$	0.394	1.185	0.175
Designed at: $35^\circ$	0.283	0.885	0.121
Designed at: $40^\circ$	0.206	0.657	0.088



## 5.7 Handover-Takeover Process: Geometrical Interpretation and Confirmation

To understand the global coverage and continuity of real-time services, the handover-takeover (known as just handover) process between two LEO satellites should be well understood, which is further geometrically interpreted and confirmed in its operation.

For tracking the satellites, real-time software fed by Kepler elements is applied. The respective software provides real-time tracking information, usually displayed in different modes. The “radar map” mode is further considered for the intended geometrical handover-takeover process interpretation. The “radar map” mode includes accurate satellite path with the ground station considered at the center, as in [Figure 5.14](#) presented what is described in details under Section 4 ([Cakaj, 2021](#)).

For LEO satellites, the maximal elevation (**Max-El**) is the main parameter of the satellite pass over the ground station (user) and determines the communication duration between LEO satellite and the respective ground station. The horizon plane with a predetermined minimal elevation is considered the **designed horizon plane**. The designed horizon

plane for users for the real-time uninterrupted communications is considered at  $40^\circ$  (usually ranges from  $25^\circ$  to  $40^\circ$ ) (Starlink, [2020](#); Starlink Satellite Missions, [2020](#)) and is presented as the thicker black circle indicated by  $40^\circ$  in the [Figure 5.14](#).

For the geometrical interpretation and confirmation purposes are identified three randomly chosen orbits, as Orbit1, Orbit2, and Orbit3, and appropriate satellite to each of them at altitudes of 550 km. For each orbit is given an arrow identifying the satellite's movement direction seen from the user. The user is located at the center. At each orbit are identified points of satellite acquisition (AOS) and satellite loss (LOS) in space. Since this is only geometrical approach, the time as a variable is not considered.

The acquisition and loss of the satellites are considered for the ideal horizon plane at ( $0^\circ$ ) and for the designed horizon plane at ( $40^\circ$ ), designated as AOS(0), AOS(40), and LOS(0), LOS(40), respectively. These events in space are determined by respective azimuth and elevation. Each of three passes is determined by its own maximal elevation, and by the appropriate azimuth. For all points indicated in [Figure 5.14](#), the coordinates are given in [Table 5.5](#) as pairs of azimuth and elevation [Az °, El °]. The values are extracted from [Figure 5.14](#), but approximated since the orbits are randomly chosen (Cakaj, [2021](#)).

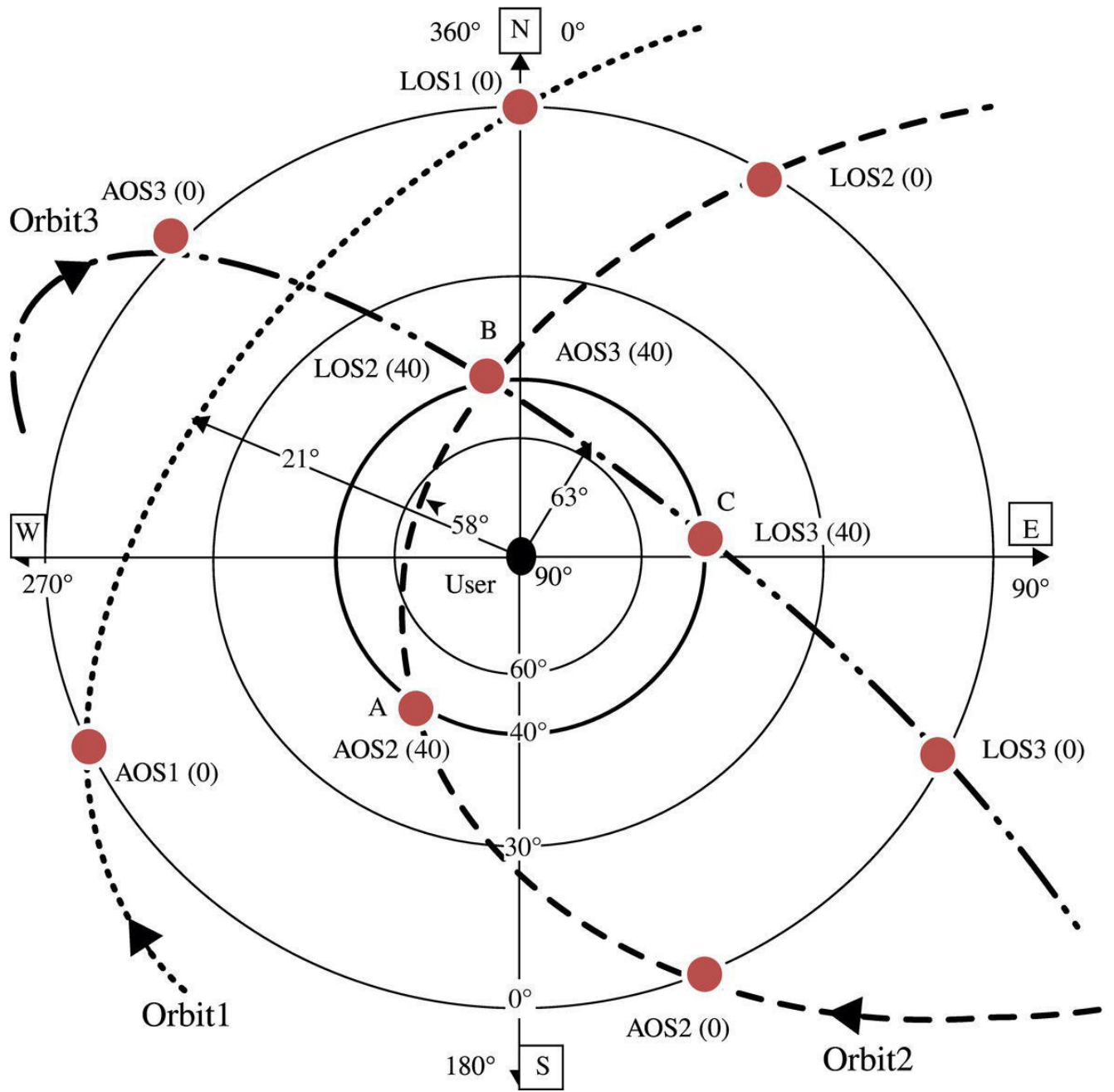


**Figure 5.14** Geometrical interpretation of the handover-takeover process.

**Table 5.5** Coordinates of the satellites space events.

Events for three orbits	Max-El	AOS (0)	AOS (40)	LOS (40)	LOS (0)
	[Az°, El°]				
Orbit1	305°, 21°	240°, 0°	NA	NA	360°, 0°
Orbit2	310°, 58°	155°, 0°	220°, 40°	345°, 40°	30°, 0°

<b>Orbit3</b>	$30^\circ, 63^\circ$	$315^\circ, 0^\circ$	$345^\circ, 40^\circ$	$85^\circ, 40^\circ$	$125^\circ, 0^\circ$
↗					

Satellite flying at Orbit1, appears at the user's ideal horizon plane approximately at azimuth of  $240^\circ$  at  $0^\circ$  elevation, noted as event AOS1(0). The satellite moves higher, achieving the Max-El of  $21^\circ$  (at Az =  $305^\circ$ ) and then down to the event LOS1(0) at coordinates [ $360^\circ, 0^\circ$ ] and disappearing from the user's ideal horizon. The user and this satellite had no communication, since the satellite is always lower than user's designed horizon plane at  $40^\circ$  ( $21^\circ < 40^\circ$ ), consequently not locked. The satellite in Orbit1, moves away unseen from the user. This fact explains NA (not applicable) of AOS (40) and LOS (40) for Orbit1 in [Table 5.5](#).

Satellite flying at Orbit2, appears at the user's ideal horizon plane approximately at azimuth of  $160^\circ$  at  $0^\circ$  elevation, noted as the event AOS2(0) but not locked with the user. Satellite moves higher to the event AOS2(40) at coordinates (Az =  $220^\circ, 40^\circ$ ) where the satellite is locked with the user establishing communication. The range between the satellite and the user at this point is 809.5 km (apply [Eq. 1.56](#)). The satellite moves higher toward Max-El event at coordinates (Az =  $310^\circ, 58^\circ$ ) still in communication with the satellite and being closest to it at the distance of 641.4 km (apply [Eq. \(1.56\)](#)). Satellite moves down, still in communication, toward the event LOS2(40) at coordinates (Az =  $345^\circ, 40^\circ$ ) having again the range of 809.5 km. At this point the satellite leaves the user's designed horizon plane and being unlocked of the communication. Satellite moves further to the event LOS2(0) at coordinates (Az =  $30^\circ, 0^\circ$ ) and leaving the user's ideal horizon plane also. For further purposes points AOS2(40) and LOS2(40) are, respectively, noted also as A and B. So, during the Orbit2, the user and the satellite had communication from point A to B, with range variation from 641.4 km to 809.5 km; consequently, one-way signal delay from 2.13 to 2.69 ms.

Satellite flying at Orbit3, appears at the user's ideal horizon plane approximately at azimuth of  $315^\circ$  at  $0^\circ$  elevation, noted as the event

AOS3(0) but not locked with the user. The satellite moves higher to the event AOS3(40) at coordinates ( $Az = 345^\circ$ ,  $40^\circ$ ) where it is locked with the user establishing communication. The range between the satellite and the user at this point is 809.5 km (apply [Eq. 1.56](#)). The satellite moves higher toward Max-El event at coordinates ( $Az = 30^\circ$ ,  $63^\circ$ ) still in communication with the satellite and being closest to it at the distance of 611.2 km. The satellite moves down, still in communication, toward the event LOS3(40) at coordinates ( $Az = 85^\circ$ ,  $40^\circ$ ) once again at the range of 809.5 km. At this point, the satellite leaves the user's designed horizon plane and is unlocked – that is, it loses communication with the ground station. Satellite moves further to the event LOS3(0) at coordinates ( $Az = 125^\circ$ ,  $0^\circ$ ) and leaving the user's ideal horizon plane, also. For further purposes points AOS3(40) and LOS3(40) are, respectively, noted also as B and C. So, during the Orbit3, the user and the satellite had communication from point B to C, with range variation from 611.2 to 809.5 km – consequently one-way signal delay from 2.03 to 2.69 ms.

The user has communication with satellite of Orbit2 from point A to B. The same user has communication with satellite of Orbit3 from point B to C. Point B, identifies the loss of the satellite in Orbit2 from the user's designed horizon plane [event LOS2(40)] and the acquisition of the satellite in Orbit3 by the user's designed horizon plane [event AOS 3(40)]. If the satellite in Orbit2 can communicate by intersatellite communication protocol with the satellite in Orbit3 at this point (zone), establishing handover-takeover process between satellites in Orbit2 and Orbit3, will be ensured uninterrupted communication between the user and the constellation from point A to C. Thus, the handover process at point B ensures the continuity of services for the user, so keeping the communication from A to C. This geometrical interpretation confirms the continuity of services by two satellites. The same applies for more of them, for satellites that can intercommunicate within appropriate constellation ([Cakaj, 2021](#)).

Just one more clarification! Seems that the satellites hit each other at point B! No way! This is a very coordinated and synchronized process. To facilitate the handover-takeover process, the LEO satellites' coverage areas overlap by a few degrees. For this process, the satellites must be adjacent to each other and able to intercommunicate (Cakaj et al., [2010](#)).

To further illustrate the handover-takeover process in space, let us assume that this process will happen at  $39^\circ$  elevation for satellite in Orbit2 (just  $1^\circ$  before leaving the user's horizon plane) and at  $41^\circ$  elevation for satellite in Orbit3 (just  $1^\circ$  before entering the user's horizon plane). The difference in  $2^\circ$  is ensured by overlapping. Can these two satellites communicate with each other to provide handover-takeover process between the satellite in Orbit2 and satellite in Orbit3? Seen from the user under  $39^\circ$ , the distance between the satellite in Orbit2 and the ground station is 827.9 km (apply [Eq. \(1.56\)](#)), ready for handover and ready to leave the designed horizon plane. On the other side, the satellite in Orbit3 at elevation  $41^\circ$  is 800.6 km (apply [Eq. \(1.56\)](#)) far from the user, ready to enter into the user's designed horizon plane and to take over the communication from the satellite in Orbit2 by itself. In these positions, the satellites can communicate. Applying cosines rule, these satellites are far from each other around 40 km in space, so they easily can communicate with each other during the handover-takeover process. Finally, this is geometrical confirmation of the handover-takeover process, which proves the continuity of real-time services by satellites, including broadband worldwide internet services.

## References

Alyildiz, I.F., Zunalioglu, H.M.D., and Bender, D.M. (1999). Handover management in low earth orbit (LEO) satellite networks. *Mobile Networks and Applications* 4 (1999): 301–310.

Cakaj, S. (2010). *Local User Terminals for Search and Rescue Satellites*, 84. Saarbrucken, Germany: VDM Publishing House.

Cakaj, S. (2016). *Coverage Belt for Low Earth Orbiting Satellites.*, 554–557. Opatija, Croatia: 39<sup>th</sup> International Convention on Information and Communication Technology, Electronics and Microelectronics, IEEE.

Cakaj, S. (2021). The parameters comparison of the “Starlink” LEO satellites constellation for different orbital shells. *Frontiers in Communications and Networks-Aerial and Space Networks* 2,, (Article ID: 643095): 1–15.

Cakaj, S., Fitzmaurice, M., Reich, J., and Foster, E. (2010). The downlink adjacent interference for low earth orbiting (LEO) search and rescue satellites. *International Journal of Communications, Networks and System Sciences (IJCNS)* 3 (2): 107–115.

Cakaj, S., Kamo, B., Lala, A., and Rakipi, A. (2014). The coverage analysis for low Earth orbiting satellites at low elevation. *International Journal of Advanced Computer Science and Applications* 5 (6): 6–10.

Cochetti, R. (2015). *Mobile Satellite Communications Handbook*, 119–155. Hoboken, NJ: Wiley Telecom.

De Selding, B.P. (2015) Virgin, Qualcomm invest in OneWeb satellite internet venture. *SpaceNews* (Jan 15).

Foust, J. (2018). Telesat to announce manufacturing plans for LEO constellation in coming months. *SpaceNews* (Feb. 18): <https://spacenews.com/telesat-to-announce-manufacturing-plans-for-leo-constellation-in-coming-months/>.

Jong, D.K., Goode, M., Liu, X. and Stone, M. (2014) Precise GNNS Positioning in Arctic Regions. *OTC Arctic Technology Conference*, Paper Number: OTC-24651-MS. Houston, Texas,

Papapetrou, P., Karapantazis, S., and Pavlidou, N.F. (2003). *Handover Policies in LEO Systems with Satellite Diversity.*, 10–11. Frascati, Italy:

International Conference on Advanced Satellite Mobile Systems (ASMS).

Pultarova, T. and Henry, C. (2017). OneWeb weighing 2000 more satellites. SpaceNews, Feb2017.

Rao, J. (2019) How to see SpaceX's Starlink satellite 'train' in the night sky. <https://www.space.com/spacex-starlink-satellites-night-sky-visibility-guide.html>

Richharia, M. (1999). *Satellite communications systems*. New York: McGraw-Hill.

Roddy, D. (2006). *Satellite communications*. New York: McGraw Hill.

Seyed, Y. and Safavi, M.S. (2012). On the analysis of random coverage time in Mobile LEO satellite communications. *Communications Letters, IEEE* 16 (5): 1–10.

Starlink (2020). [https://en.wikipedia.org/wiki/Starlink#Global\\_broadband\\_Internet](https://en.wikipedia.org/wiki/Starlink#Global_broadband_Internet) (Accessed January 17, 2021).

Starlink Satellite Missions (2020). <https://directory.eoportal.org/web/eoportal/satellite-missions/s/starlink> (Accessed January 17, 2021).

Xiao, Y., Zhang, T., and Liu, L. (2018). Addressing subnet division based on geographical information for satellite-ground integrated network. *IEEE Access*, PP (99): 1–1. DOI:10.1109/ACCESS.2018.2882594. <https://ieeexplore.ieee.org/document/8546744>.

Zong, P. and Kohani, S. (2019). Optimal satellite LEO constellation design based on global coverage in one revisit. *International Journal of Aerospace Engineering*. <https://doi.org/10.1155/2019/4373749>.

# 6

## LEOs Sun Synchronization

### 6.1 Orbital Sun Synchronization Concept

Earth is our home planet. The Earth rotates west to east, known as a *prograde direction*. Humans have known that the Earth is round for more than 2000 years! Even though our planet is a sphere, shown in [Figure 6.1](#), it is not a perfect sphere (NASA. What is the Earth? [2020](#)). Earth daily rotates at around 1000 mph (Gunn [2020](#)). Earth's rotation, wobbly motion, and other forces are very slowly changing the planet's shape, flattening at the poles and bulging at the equator, but still keeping the roundish shape as an *oblate ellipsoid*, shown in [Figure 6.2](#) (Knippers [2009](#)).

An orbit in which one satellite moves in the same direction as the Earth's rotation is known as *prograde* or *direct orbit*. The inclination of a prograde orbit always lies between  $0^\circ$  and  $90^\circ$ . Most satellites are launched in a prograde orbit because the Earth's rotational velocity provides part of the orbital velocity, saving launch energy (Richharia [1999](#); Roddy [2006](#); Maral and Bousquet [2005](#)). An orbit in which the satellite moves in direction opposite to that of the Earth's rotation is called *retrograde orbit*. The inclination of a retrograde orbit always lies between  $90^\circ$  and  $180^\circ$ . Sun synchronized orbits (SSOs), further discussed, are typically retrograde.

Microsatellites in low Earth orbits (LEOs) have been used for the last three decades, including for communications and scientific purposes. This chapter is dedicated mostly to scientific applications related to space observation and environmental monitoring.

[Figure 6.3](#) gives an example of weather monitoring from satellites (ESA, Cyclone, west of Madagascar [2019](#)). Such scientific missions are permanently developing, especially in fields where similar experiments by purely Earth-based means are now impracticable or too difficult to be implemented – including meteorology, oceanography, agriculture, biodiversity, forestry, landscape, geology, cartography, regional planning, education, intelligence, defense, and military.

These missions are mainly based on photo imagery records. The Sun's position is very important for photo imagery; thus, the observed area from the satellite to be treated under the same lighting (illumination) conditions. This can be achieved by keeping the orbital plane position constant relative to the Sun due to the Earth's motion around the Sun, what means that the satellite will observe a location on Earth at the same daily time, known as the Sun synchronization process, which is applicable only for LEO orbits.

Having these images under the same illumination conditions, of the different times, enables scientists or appropriate businesses to compare images and conclude about changes over time. Therefore, scientists use image series like these to investigate how weather patterns emerge, to help predict weather or storms; when monitoring emergencies like forest fires or flooding; or to accumulate data on long-term problems like deforestation or rising sea levels (Polar and Sun synchronous orbit 2020). As better quality of the images the better scientific outcomes. On this trend, Pleiades Neo satellite optical constellation with four identical 30 cm resolution Sun synchronized satellites provides top-level Earth observation services now and going forward into decades to come ([Pléiades Neo constellation 2021](#)).



**Figure 6.1** Earth rotating.

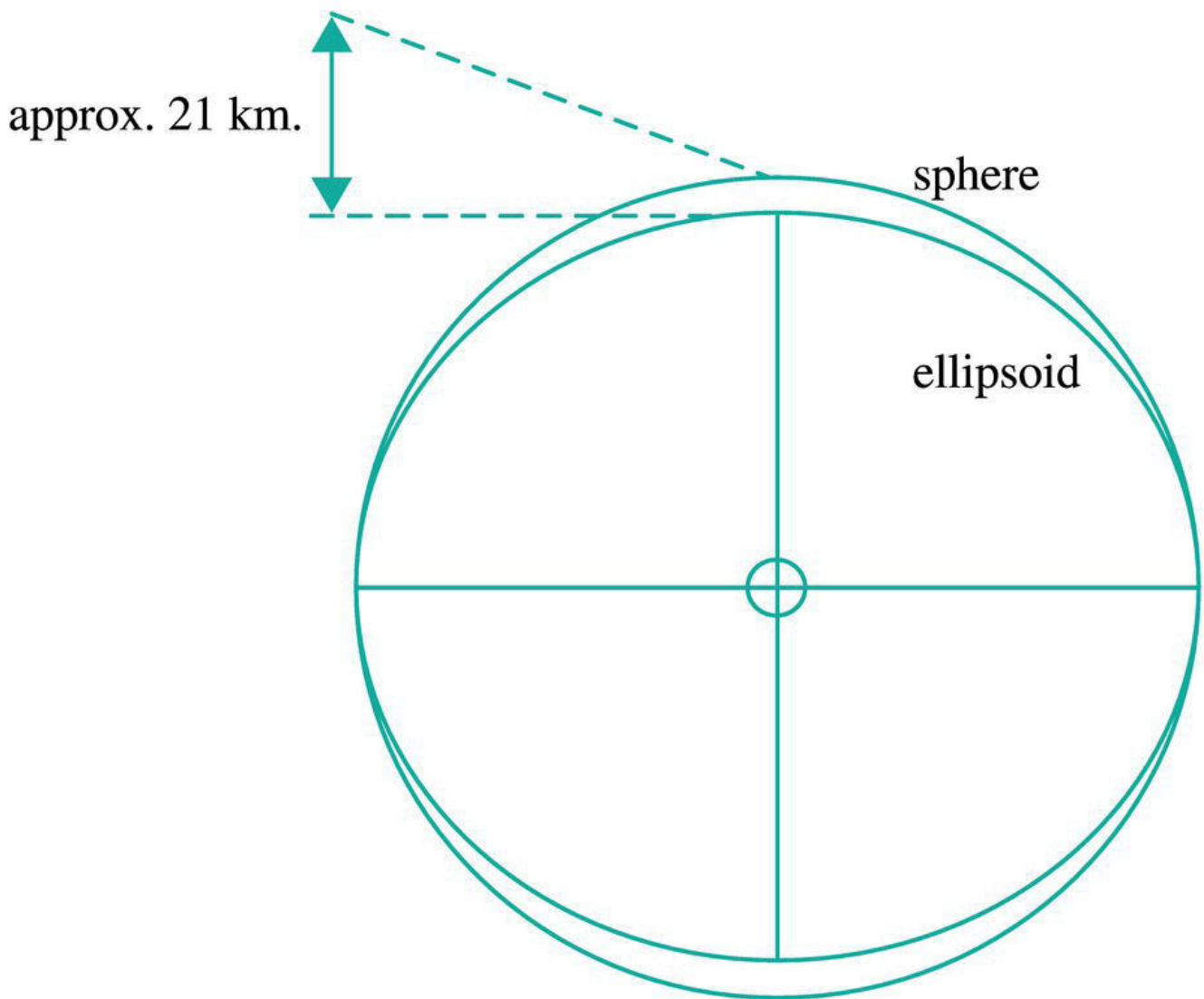


**Figure 6.2** Earth's oblateness.

How are orbits synchronized with the Sun? The Earth is not a perfectly spherical homogeneous body. It is a round body characterized by a bulge at the equator, and a slight flattening at the poles. Due to the irregularities of Earth's rotation and not homogenous Earth's mass distribution, the terrestrial potential at a point in space (in our case, the point indicates a satellite) depends not only on the distance  $r$  to the Earth's center but also on the respective longitude and latitude of the appropriate point within a spherical coordinate system. The terrestrial potential has been well studied by Kozai (1964) and then by Goddard Space Flight Center, which developed “Goddard Earth Models,” denoted as GEM-1, GEM-2, GEM-3, and GEM-4 (Geopotential model 2022, Maral and Bousquet 2005). For both the Kozai and Goddard approaches, it is common to express the

terrestrial potential in terms of geopotential zonal harmonic coefficients  $J_n$ . The  $J_2$  term due to flattening of the Earth (about 21 km, [Figure 6.2](#)) dominates all other harmonics. Based on Kozai ([1964](#)) and Maral and Bousquet ([2005](#)), the  $J_2$  harmonic is nondimensional value given as:

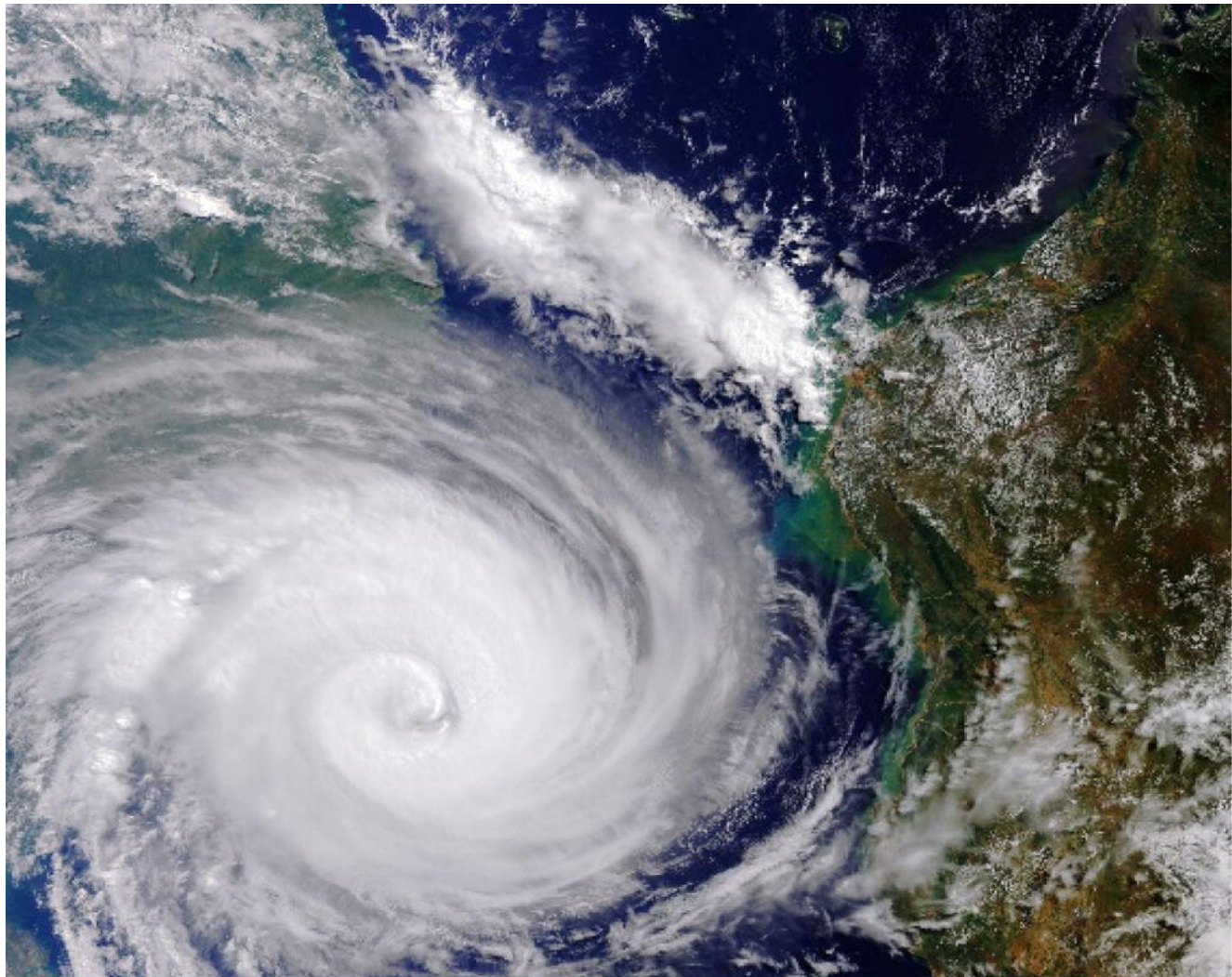


[Figure 6.3](#) Cyclone, west of Madagascar (ESA [2019](#)).

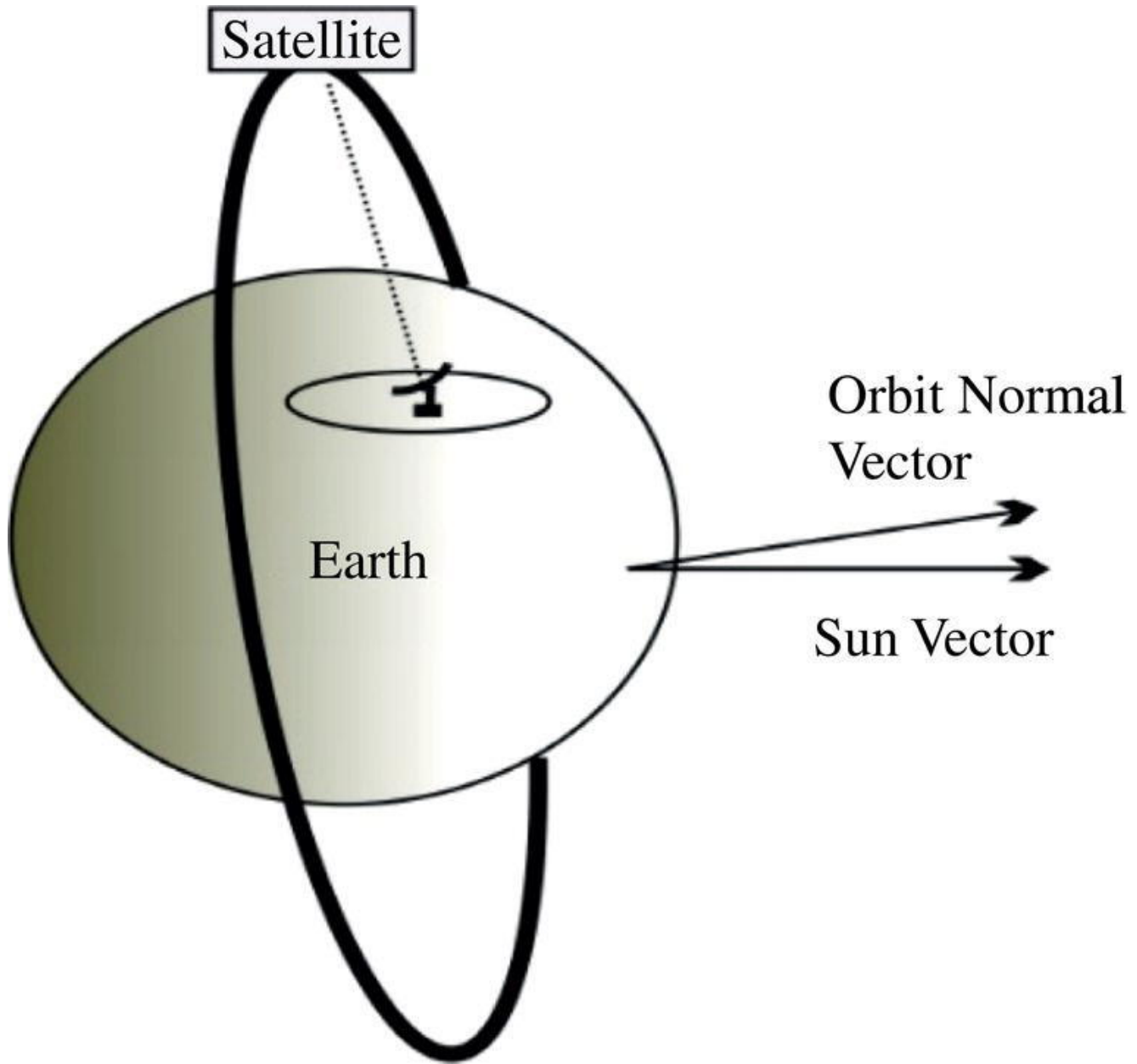


**Figure 6.4** Orbital Sun synchronization concept.

$$J_2 = 1.0827 \cdot 10^{-3} \quad (6.1)$$

For missions accomplished based on photo imagery, in order to keep and treat the observed area under the same illumination conditions due to the different satellite paths over the observed area on the Earth, somehow the orbit (orbital plane) should be managed (controlled) to keep the same position related to the Sun. Geometrically, this could be interpreted as keeping a constant angularity between the orbital plane and the Sun, or better defined, keeping constant angularity between the perpendicular (normal) vector on the orbital plane and the Sun direction vector, as given

in [Figure 6.4](#) (Cakaj et al. 2009). Since the Earth's rotation around the Sun takes one year, for consistency purposes, the orbit should maintain the appropriate position relative to Sun throughout the various seasons of the year, as presented in [Figure 6.5](#) (Richharia 1999; Roddy 2006; Maral and Bousquet 2005). Orbits that fulfill this condition are known as Sun Synchronized Orbits (SSOs).

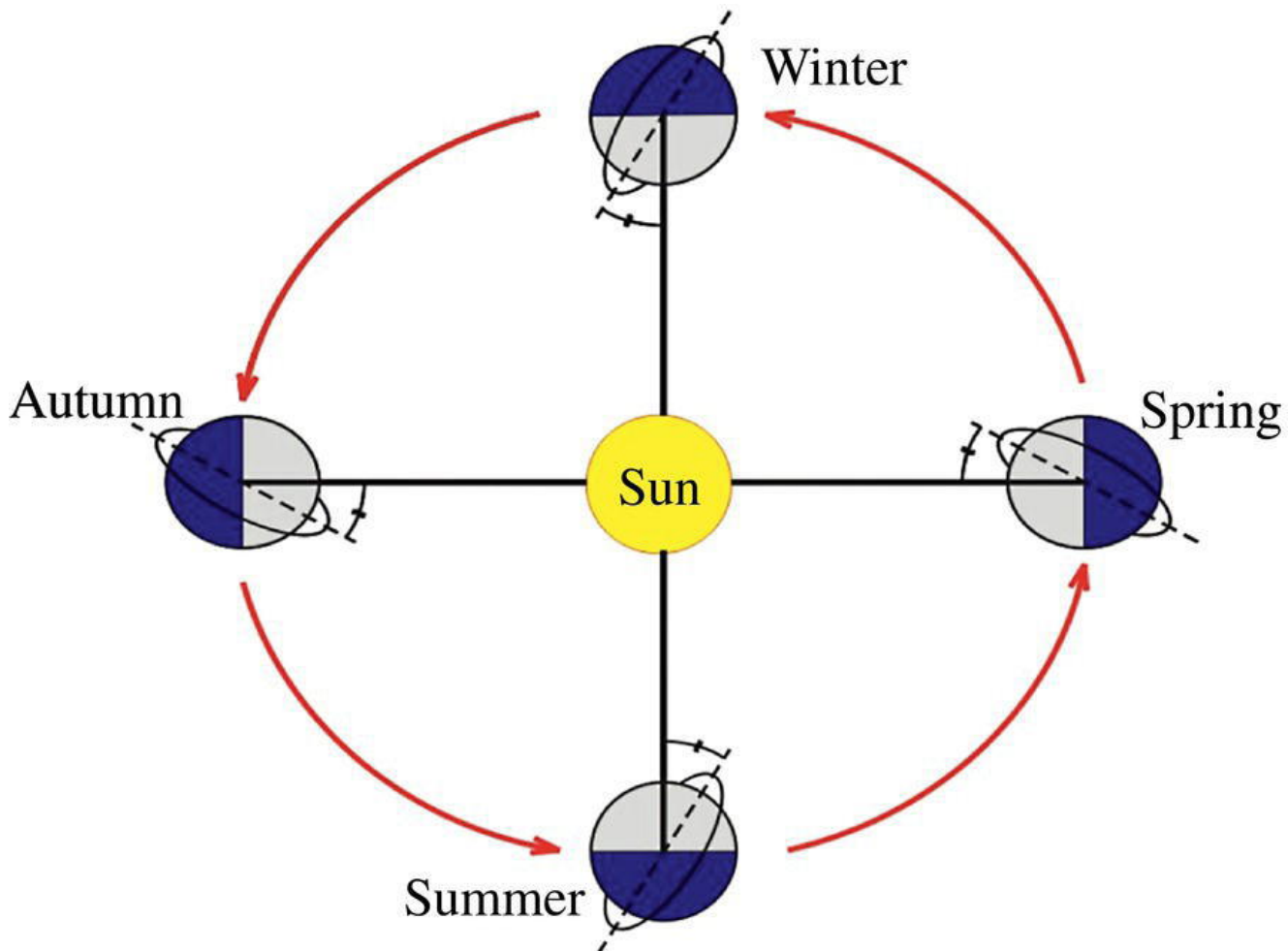


[Figure 6.5](#) Seasons Sun synchronization.

To a first approximation, the orbital plane is fixed in space as the satellite orbits around the Earth. But, due to the different potentials generated by the non-spherical Earth, at different orbital points in space, variations of the orbital elements happen. The most affected orbital elements are *ascending/descending nodes* and the *argument of perigee*, as presented in [Figure 4.2](#). The affected ascending/descending nodes consequently affect the line of nodes, creating a drift of the orbital plane. Let us first discuss

the effect on *ascending/descending nodes (line of nodes)* and later on the argument of perigee deviation.

From [Figure 4.2](#), we see that the line of nodes represents the intersection line (interconnecting ascending node, Earth's center, and descending node) between equatorial plane and the orbital plane. Line of nodes is determined by the right ascension of ascending node ( $\Omega$ ) of the orbital plane, as in [Figure 4.2](#). If the orbital plane drifts because of nonuniform terrestrial potential, so will the line of nodes, manifested as the slide of line of nodes on the equatorial plane always drifting around the Earth's center, as the central point of the line of nodes. This line of nodes shifting around the Earth's center on the equatorial plane, because of Earth's oblateness and nonhomogeneous mass, is known as the *nodal regression*.

## 6.2 Orbital Nodal Regression

The line of nodes determines the orientation of the satellite's orbital plane in space. Nodal regression refers to the shift of the orbit's line of nodes over time as Earth revolves around the Sun, due to the Earth's oblate nature. Nodal regression is an especially useful feature for the low circular orbits providing to them the Sun synchronization. A Sun-synchronized orbit lies in a plane that maintains a fixed angle with respect to the Earth–Sun direction. Nodal regression depends on orbital altitude and orbital inclination angle. In the low Earth, Sun synchronized circular orbits are suited satellites that accomplish their photo imagery missions. If the orbit is prograde, the line of nodes slides westward, and if it is retrograde, it slides eastward. This means that nodes (line of nodes) move in opposite direction to the direction of satellite motion, hence the term *nodal regression*.

For the LEO, determined by semimajor axis  $a$  and its eccentricity  $e$  laid on the orbital plane in space, which is determined by inclination  $i$  and the right ascension of the ascending node  $\Omega$ , an approximate expression

for the nodal rate regression of  $\Omega$  due to time is expressed as (Maral and Bousquet [2005](#)):

$$\frac{d\Omega}{dt} = - \left( \frac{3}{2} \right) n_0 A J_2 \cos i \quad (6.2)$$

where  $J_2$  is the second harmonic of the terrestrial geopotential, and  $n_0$  is mean satellite movement:

$$n_0 = \frac{2\pi}{T} \quad (6.3)$$

where  $T$  is orbital period. Furthermore,  $A$  is constant given as:

$$A = \frac{R_E^2}{a^2(1-e^2)^2} \quad (6.4)$$

$R_E = 6378$  km is Earth's radius,  $e$  is orbital eccentricity,  $i$  is the inclination, and  $a$  is a semimajor axis of satellite's orbit.

For circular orbits, approximately  $e = 0$  and  $a = r$ , where  $r$  is orbital radius of circular orbit. Orbital period for circular orbits is expressed as:

$$T = 2\pi \sqrt{\frac{r^3}{\mu}} \quad (6.5)$$

where  $\mu = 3.986005 \cdot 10^5$  km<sup>3</sup>/s<sup>2</sup> is Earth's geocentric gravitational constant. For circular orbit yields out:

$$A = \frac{R_E^2}{r^2} \quad (6.6)$$

Substituting  $R_E$ ,  $\mu$  and  $J_2$ , finally results in nodal regression expressed by inclination  $i$  and orbital radius  $r$ . The nodal regression expressed in (°/day) is (Cakaj et al. [2013](#)).

$$\Delta\Omega = -2.06474 \cdot 10^{14} \cdot \frac{\cos i}{r^{7/2}} [^\circ/\text{day}] \quad (6.7)$$

From [Eq. \(6.7\)](#), the nodal regression for circular orbits depends on orbit inclination and orbital altitude (radius). The nodal regression becomes zero in the case of the inclination angle being  $90^\circ$ . When the orbit inclination angle is  $i < 90^\circ$ , then deviation is negative, so according to [Eq. \(6.2\)](#) the satellite orbital plane rotates in a direction opposite to the direction of the Earth's rotation.

When the orbit inclination angle is  $i > 90^\circ$ , then deviation is positive, so the satellite orbital plane rotates in the same direction as the direction of the Earth's rotation. From the above statements we see that if the orbit is prograde (eastward), the nodes slide westward, and if it is retrograde (westward), the nodes slide eastward. Thus, nodes (line of nodes) move in the opposite direction to the direction of satellite motion, hence the term *nodal regression*.

**Idea:** Considering the [Eq. \(6.2\)](#) or [Eq. \(6.7\)](#), the idea is to draw conclusions about the range of nodal regression under different altitudes and inclination.

**Method:** Consider Van Allen belt effect (Van Allen radiation belt [2020](#)) for simulation purposes at attitudes from 600 up to 1200 km. LEOs have very low eccentricity, which can be considered  $e \approx 0$  and then  $a = r$ . Thus, for altitudes from 600 up to 1200 km and considering Earth's radius as  $R_E \approx 6400$  km, the orbits' radius range is 7000 to 7600 km.

**Results:** Considering [Eq. \(6.7\)](#) for these orbits and assumed radius ranges, the nodal regression [ $^\circ/\text{day}$ ] for different inclination angles  $i$  are calculated and presented in [Table 6.1](#) and [Figure 6.6](#). [Figure 6.6](#), shows that for the eastward regression, inclination  $i$  must be greater than  $90^\circ$ ; consequently, the orbit must be retrograde. This feature enables an orbital plane to stay in constant angular relationship with the Sun throughout the seasons, which will be proved by the next section.

The nodal regression is inversely dependent on  $r^{-7/2}$ . Considering the LEO satellite altitude of 1200 km, the nodal regression is around  $6.7^\circ$ . Considering MEO altitudes of 10 000 km, around 10 times more than LEO altitudes, applying the [Eq. \(6.7\)](#), the nodal regression is almost negligible. This means that medium or geosynchronous orbits cannot be Sun synchronized.

**Table 6.1** Nodal regression ( $^\circ/\text{day}$ ).

Inclination [ $^\circ$ ]	Orbital radius [km]			
	7000	7200	7400	7600
20	-6.74	-6.12	-5.55	-5.06
30	-6.21	-5.64	-5.12	-4.66
40	-5.50	-4.99	-4.52	-4.13
50	-4.61	-4.19	-3.78	-3.46
60	-3.59	-3.26	-2.95	-2.69
70	-2.45	-2.22	-2.02	-1.84
80	-1.24	-1.13	-1.02	-0.94
90	0	0	0	0
100	1.24	1.13	1.02	0.94
110	2.45	2.22	2.02	1.84
120	3.59	3.26	2.95	2.69
130	4.61	4.19	3.78	3.46
140	5.50	4.99	4.52	4.13
150	6.21	5.64	5.12	4.66
160	6.74	6.12	5.55	5.06



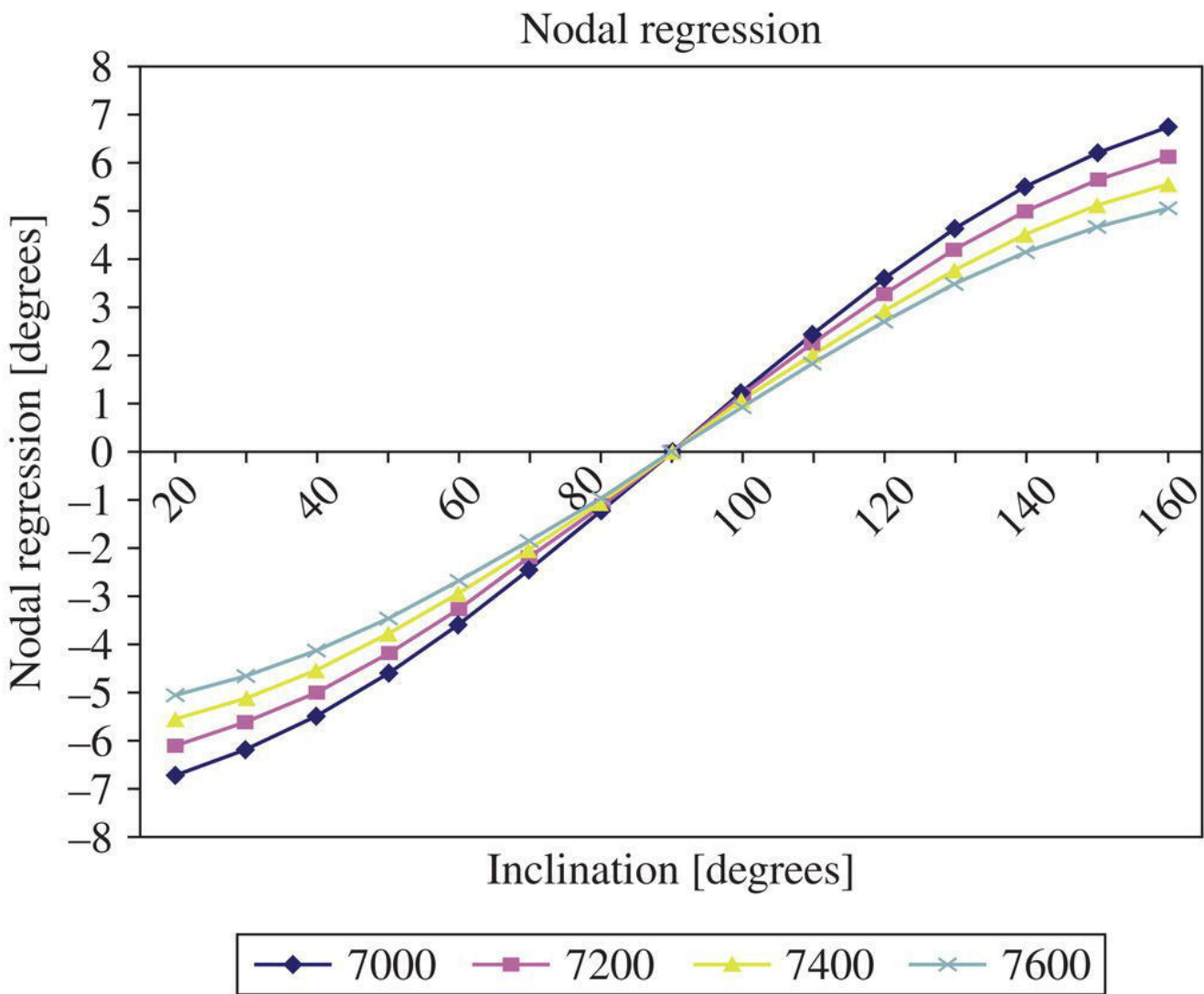


**Figure 6.6** Nodal regression [ $^{\circ}$ /day].

**Conclusion:** These results confirm that nodal regression for attitudes from 600 up to 1200 km may range from  $0^{\circ}$  up to  $6.7^{\circ}$ , depending on inclination angle. Lower inclination causes higher deviation. For inclination of  $90^{\circ}$ , there is no nodal deviation. Only LEOs can be Sun synchronized; thus, the photo imagery mission can be accomplished only by LEO satellites, to provide high performance.

### 6.3 LEO Sun Synchronization and Inclination Window

[Section 6.2](#) defined the correlation between line of nodes deviation ( $d\Omega$ ) over time and inclination. The sign (-) is because of the opposite direction

of the satellite's motion and the nodal deviation (nodal regression). This is the feature, applied for Sun-synchronization. But how?

An orbital plane fixed with respect to the Earth effectively makes a  $360^\circ$  rotation in space in a year (about 365.25 days), since Earth itself rotates by  $360^\circ$  around the Sun. This rate is equivalent to a rotation of the orbital plane of about  $0.986 [{}^\circ/\text{day}]$  (Cakaj et al. [2009](#)). By choosing a pair of particular values of  $i$  and  $r$ , it is possible to obtain an orbit for which the nodal regression varies each day by a quantity equal to the rotation of the Earth around the Sun. Mathematically, this is expressed as:

$$\frac{d\Omega}{dt} = 0.9856 {}^\circ/\text{day} \quad (6.8)$$

Applying [Eq. \(6.8\)](#) at [\(6.7\)](#):

$$\Delta\Omega = -2.06474 \cdot 10^{14} \cdot \frac{\cos i}{r^{7/2}} = 0.9856 [{}^\circ/\text{day}]. \quad (6.9)$$

From this equation it follows that for eastward regression, inclination  $i$  must be greater than  $90^\circ$ ; thus, the orbit should be retrograde. [Figure 6.7](#) shows the SSO, which obviously has an inclination  $i$  greater than  $90^\circ$  (Sunsynchronous orbit [2019](#)). A satellite in a Sun-synchronous orbit would usually be at an altitude of between 600 and 800 km.

Under the condition expressed by [Eq. \(6.8\)](#), the angle between perpendicular vector on the orbital plane and the Sun direction vector remains constant throughout the year, or having the constant angularity during the year. This feature is known as LEO Sun synchronization. It is confirmed through the previous section that only LEOs can be Sun synchronized.

**Idea:** The further question is, what is the inclination window for LEO Sun synchronization for the range of altitudes for LEO orbits?

**Method:** Mathematics and simulation are applied. By solving the [Eq. \(6.8\)](#), for orbital altitude of 600 km consequently for  $a = r = 7000$  km under no eccentricity ( $e = 0$ ) will get inclination for Sun synchronization as:

$$i_1 = 97.9 \quad (6.10)$$

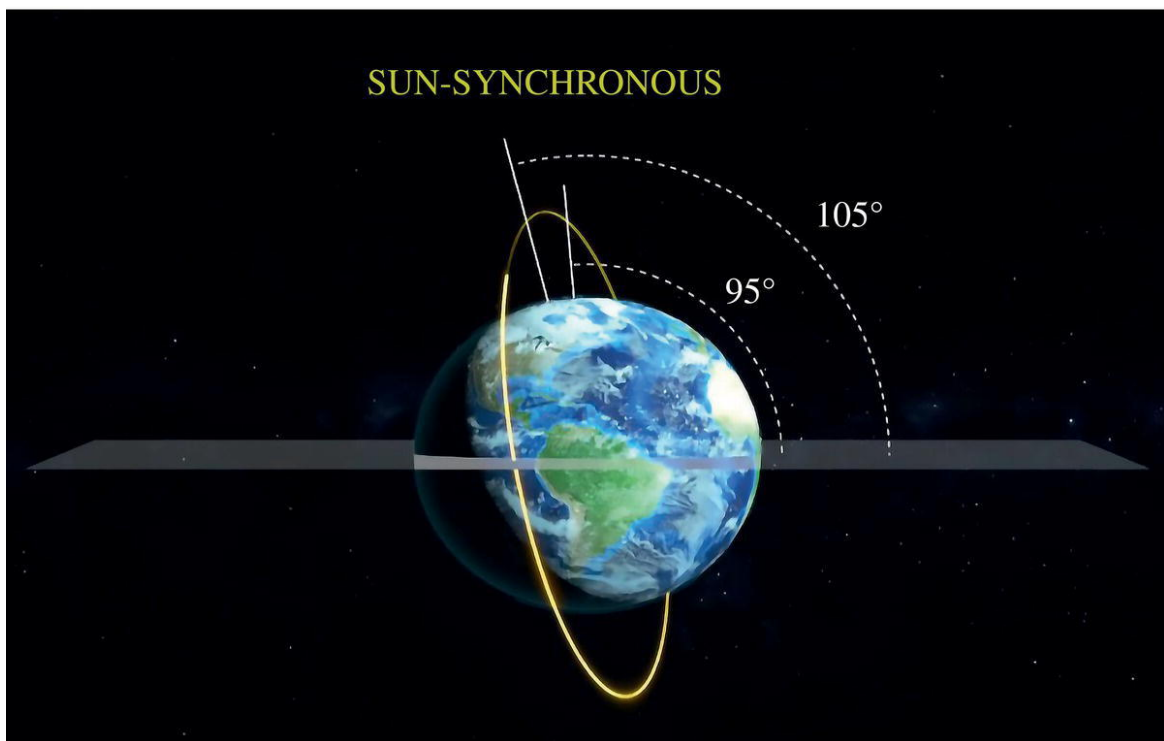


**Figure 6.7** Sun synchronized orbit (SSO).

and for orbital attitude of 1200 km consequently for  $a = r = 7600$  km under no eccentricity ( $e = 0$ ) will get inclination for sun synchronization as:

$$i_2 = 100.5^\circ. \quad (6.11)$$

Further, considering these values of inclination, but also the range for lower and higher orbital attitudes (600–1200 km), the nodal regression for the inclination from  $97^\circ$  up to  $101^\circ$  (Sun-synchronized inclination window) is calculated.

**Results:** These results are given in [Table 6.2](#) and [Figure 6.8](#) (Cakaj et al. 2013).

In [Figure 6.8](#) the nodal regression of  $0.986[\text{°}/\text{day}]$  in fact represents the daily angular rotation of the Earth around the Sun.

**Conclusion:** Sun-synchronization for LEO circular orbits depend on altitude and inclination. SSOs are retrograde. The orbital Sun synchronization is achieved through inclination angle at range of  $97.9\text{--}100.5^\circ$  for LEO altitudes from 600 to 1200 km. The inclination window for Sun synchronization has a width of  $2.6^\circ$  for altitudes of 600 to 1200 km. A Sun-synchronization feature is typical for LEOs. At medium and high orbits (MEO or GEO), the nodal regression effect is negligible, so these orbits could not be Sun synchronized.

**Table 6.2** Nodal regression for sun-synchronized inclination window ( $^\circ/\text{day}$ ).

Inclination [ $^\circ$ ]	Orbital radius [km]			
	7000	7200	7400	7600
97	0.876	0.793	0.721	0.656
98	1.001	0.906	0.824	0.750
99	1.125	1.018	0.926	0.843
100	1.248	1.131	1.028	0.936
101	1.372	1.242	1.129	1.028



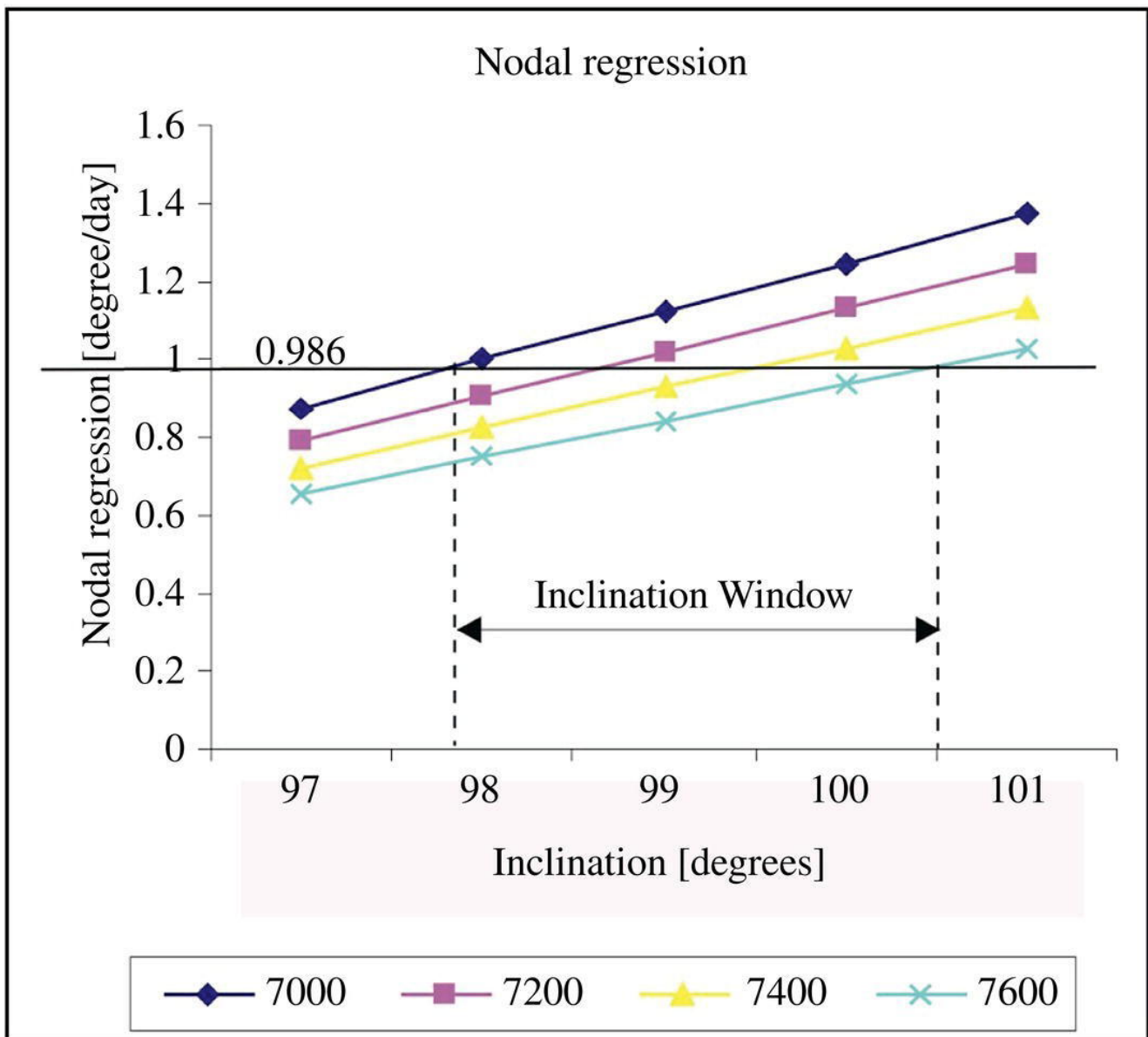


**Figure 6.8** Inclination window.

## 6.4 Perigee Deviation under Inclination Window for Sun-Synchronized LEOs

The orientation of the orbit within orbital plane is defined by the *argument of perigee*  $\omega$  ([Figure 4.2](#)) The argument of the perigee determines the position of the major axis. This is the angle, taken positively from  $0^\circ$  to  $360^\circ$  in the direction of the satellite's motion, between the direction of the line of nodes and the direction of the orbital perigee. Like the line of nodes shifting due to equatorial bulge of Earth,

the argument of perigee undergoes natural perturbation, also. This is defined as ***orbital perigee deviation***.

**Idea:** The further idea is to calculate this orbital perigee deviation for Sun-synchronized orbits, or better, saying how much the major axis deviates for one satellite pass for Sun-synchronized orbits. This perturbation may be visualized as the movement of the elliptical orbit in a fixed orbital plane, as presented in [Figure 6.9](#) (Figure presents the case of only perigee deviation under unchangeable line of nodes position). This deviation happens in a fixed orbital plane (two orbits in [Figure 6.9](#) lie in the same plane; it is in fact an original and a deviated orbit). Obviously, the apogee and perigee points change in position, manifested as a major axis drift, deviated by  $\Delta\omega$ . The question is, how much?

**Method:** Mathematics and simulation are applied. For analytical and simulation purposes, the altitudes from 600 to 1200 km are considered. Further, to determine perigee deviation under inclination window of the Sun-synchronized orbits, we simulate the orbital perigee deviation for the considered altitudes and the eventual impact on the satellite's mission. This deviation is a function of the satellite altitude and orbital plane inclination angle. This drift is analyzed under all serious satellite books, and for simulation purposes is applied here ([Maini and Agrawal 2011](#), p. 83), expressing the perigee deviation per orbit in [°/orbit] as:

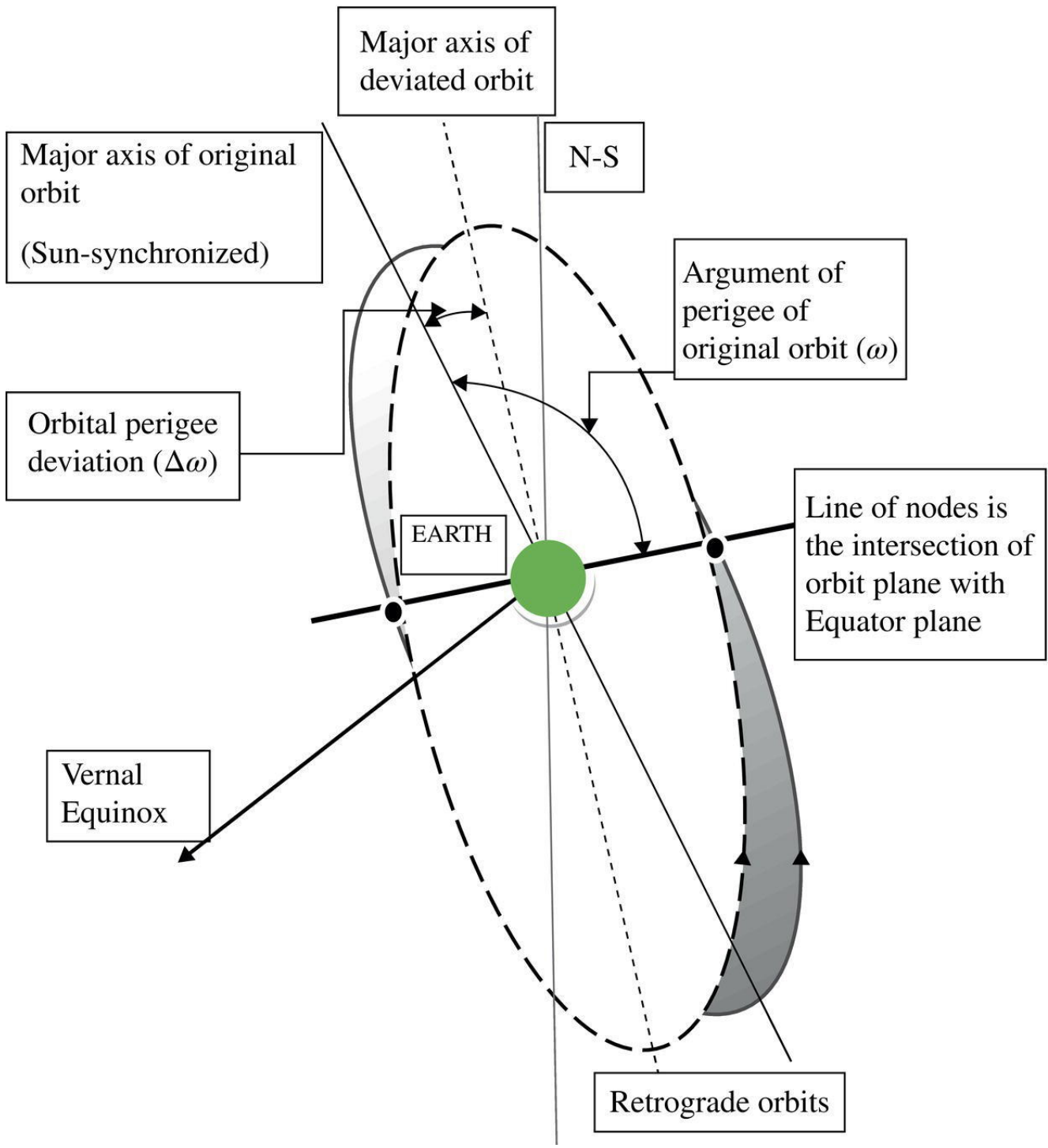


**Figure 6.9** Orbital perigee deviation.

$$\Delta\omega = 0.29 \left[ \frac{4 - 5 \sin^2 i}{(1 - e^2)^2} \right] \left[ \left( \frac{D}{r_a + r_p} \right)^2 \right] \quad (6.12)$$

This is the general expression for elliptical orbit, where  $i$  is inclination,  $e$  is orbit eccentricity,  $r_a$ ,  $r_p$  are orbital apogee and perigee, and  $D$  is Earth's

diameter. Based on [Eq. \(6.12\)](#), there is no perigee deviation under the inclination of  $63.4^\circ$  (the feature is applied for Molnya orbit) since:

$$4 - 5 \sin^2(63.4^\circ) = 0 \rightarrow \Delta\omega = 0 \quad (6.13)$$

For the inclination lower than  $63.4^\circ$ , then,  $\Delta\omega$  is positive, so the perigee deviation occurs in the same direction as the satellite motion, and for the inclination greater than  $63.4^\circ$ ,  $\Delta\omega$  is negative, so the perigee deviation occurs in the opposite direction as the satellite's motion. Also, the closer the satellite is to the center of the Earth, the larger is the deviation.

For simulation purposes, consider altitudes from 600 to 1200 km, and Earth's radius as  $R_E \approx 6400$  km; then the orbits' radius ranges from 7000 to 7600 km. From the previous section, based on [Eq. \(6.9\)](#), we know that the range of orbital inclination lies from  $97.9^\circ$  to  $100.5^\circ$  to attain Sun synchronization (Cakaj et al. [2013](#)). The inclination within this range is always greater than  $63.4^\circ$ ; thus, the result of [Eq. \(6.12\)](#) is always negative, which means that the orbital major axis will drift in the opposite direction to the satellite's motion.

LEO are usually circular orbits, so the eccentricity is 0. Also,  $r_a = r_p = a$ , where  $a$  is a semi-major axis and  $D = 2R_E$ , where  $R_E \approx 6400$  km is Earth's radius. Applying these statements at [Eq. \(6.12\)](#), yields the perigee deviation for low Earth Sun-synchronized orbits.

$$\Delta\omega = 0.29 \left( \frac{R_E}{a} \right) [4 - 5 \sin^2 i] \quad (6.14)$$

For Sun-synchronization, the orbital inclination lies on range:

$$97.9^\circ \leq i \leq 100.5^\circ \quad (6.15)$$

Finally, the orbital perigee deviation for any Sun-synchronized orbit lies in the range of:

$$\Delta\omega_{(i=97.9)} \leq \Delta\omega \leq \Delta\omega_{(i=100.5)} \quad (6.16)$$

**Results:** The calculation of orbital perigee deviation and appropriate results are presented in [Table 6.3](#) (Cakaj and Kamo [2019](#)).

The negative sign indicates that the orbital perigee deviation shifts in opposite side to the satellite motion. From the [Table 6.3](#), it is obvious that the largest perigee deviation appears at altitude of 7000 km at inclination of  $97.9^\circ$  and the lowest perigee deviation appears at altitude of 7600 km at inclination of  $100.5^\circ$ . These values converted in minutes, represent the deviation of  $13.1'$  and  $10.3'$  per orbit, respectively, for the largest and lowest case.

Finally, the orbital perigee deviation expressed in [ $^\circ/\text{orbit}$ ], for LEO Sun-synchronized orbits is mathematically expressed as Cakaj and Kamo ([2019](#)):

$$10.3' \leq \Delta\omega \leq 13.1' \quad [^\circ/\text{orbit}] \quad (6.17)$$

This calculation leads toward the thrust vector being applied in order to keep argument of perigee under a predefined value, respectively unchangeable over time. The vector intensity depends on absolute value of perigee deviation.

**Conclusion:** Sun-synchronized orbits are very useful for Earth's observation (scientific satellites) applications. Nodal regression is especially utilized for LEO circular orbits, providing them Sun synchronization. SSOs are always retrograde because the inclination is greater than  $90^\circ$ . Due to Earth's equatorial bulge and natural perturbations, the argument of the perigee also deviates. This is known as orbital perigee deviation, expressed in  $^\circ/\text{orbit}$ . For the considered LEO altitudes under the Sun synchronized inclination window, the orbital perigee deviation ranges from 10.3 to 13.1 ('/orbit), always in the opposite direction of the satellite motion.

**Table 6.3** Perigee deviation for Sun-synchronized orbits.

Inclination [°]	Orbit radius [km]			
	7000	7200	7400	7600
97.9	-0.219	-0.207	-0.196	-0.186
100.5	-0.202	-0.191	-0.180	-0.171



## References

Cakaj, S. and Kamo, B. (2019). Orbital perigee deviation under inclination window for Sun synchronized low Earth orbits. *EJERS, European Journal of Engineering Research and Science* 4 (10) Brussels: 127–130.

Cakaj, S., Fischer, M., and Schotlz, L.A. (2009). Sun Synchronization of Low Earth Orbits (LEO) through Inclination Angle. In: *28th IASTED International Conference on Modelling, Identification and Control, MIC 2009*, Innsbruck, Austria, 155–161.

Cakaj, S., Kamo, B., and Malaric, M. (2013). The inclination window for low Earth sun synchronized satellite Orbits. *Transactions on Maritime Science* 2 (1) Split, Croatia: 15–19.

ESA, Cyclone, west of Madagascar, (2019). [https://www.esa.int/ESA\\_Multimedia/Images/2019/03/Cyclone\\_Idai\\_west\\_of\\_Madagascar](https://www.esa.int/ESA_Multimedia/Images/2019/03/Cyclone_Idai_west_of_Madagascar)

Geopotential model (2022). [https://en.wikipedia.org/wiki/Geopotential\\_model](https://en.wikipedia.org/wiki/Geopotential_model)

Gunn, A. (2020). What is the speed rotation! *Science Focus* <https://www.sciencefocus.com/planet-earth/earth-rotation-speed.>

Knoppers, R. (2009). *Geometric Aspects of Mapping*. Enschede, The Nederland: International Institute for Geo-Information Science and Earth Observation (ITC).

Kozai, Y. (1964). New determination of zonal harmonics coefficients of the earth's gravitational potential. *Astronomical Society of Japan* 16: 263. Bibliographic Code: 1964PASJ...16...263K.

Maini, K.A. and Agrawal, V. (2011). *Satellite Technology*, 2e. West Sussex: Wiley.

Maral, G. and Bousquet, M. (2005). *Satellite Communications Systems*, 4e. West Sussex: Wiley.

NASA (2020). What is the Earth? <https://www.nasa.gov/audience/forstudents/5-8/features/nasa-knows/what-is-earth-58.html>

Pléiades Neo constellation (2021). [https://www.intelligence-airbusds.com/imagery/constellation/pleiades-neo/?gclid=EAIAIQobChMI1\\_2\\_tdPZ9QIV1uFRCh0IRQIhEAAYASAAEgIzJ\\_D\\_BwE](https://www.intelligence-airbusds.com/imagery/constellation/pleiades-neo/?gclid=EAIAIQobChMI1_2_tdPZ9QIV1uFRCh0IRQIhEAAYASAAEgIzJ_D_BwE)

Sunsynchronous orbit (2019) <https://uzayteknesi.com/2019/11/30/yorunge-tipleri-sun-synchronous-orbit/>

Richharia, M. (1999). *Satellite Communications Systems*. New York: McGraw Hill.

Roddy, D. (2006). *Satellite Communications*, 4e. New York: McGraw Hill.

Van Allen radiation belt. [https://en.wikipedia.org/wiki/Van\\_Allen\\_radiation\\_belt](https://en.wikipedia.org/wiki/Van_Allen_radiation_belt).